A Design Optimization Framework for Enhanced Compressor Stability Using Dynamic System Modeling

by

Vincent P. Perrot

Submitted to the Department of Aeronautics and Astronautics
in partial fulfillment of the requirements for the degree of

MASTER OF SCIENCE IN AERONAUTICS AND ASTRONAUTICS

at the

MASSACHUSETTS INSTITUTE OF TECHNOLOGY

September 2003

Author_____
Department of Aeronautics and Astronautics
August 22, 2003

Certified by_____
Professor Zoltán S. Spakovszky
C.R. Soderberg Assistant Professor of Aeronautics and Astronautics
Thesis Supervisor

Accepted by_____
Professor Edward M. Greitzer
H.N. Slater Professor of Aeronautics and Astronautics
Chair, Committee on Graduate Students

A Design Optimization Framework for Enhanced Compressor Stability Using Dynamic System Modeling

by

Vincent P. Perrot

Submitted to the Department of Aeronautics and
Astronautics on August 22, 2003, in partial fulfillment of the
requirements for the degree of
Master of Science in Aeronautics and Astronautics

Abstract

This thesis constitutes the second year effort of a joint engineering project initiated in 2001 by Snecma Moteurs, ENSAE, ECL and MIT. The long term objective of this joint project is to conceive, design, implement and operate an advanced core compressor for an unmanned air vehicle. This thesis addresses the issue of compressor design in the light of enhanced stability, introducing a novel approach with respect to industry-practice: compressor dynamic stability is to be considered as a prime design variable.

This present study focuses on the development and implementation of a compressor design optimization framework for enhanced stability based on an existing reduced order dynamic system modeling approach [15]. Stall margin, a common metric for compressor stability, is chosen as an optimization objective in the light of performance constraints. Modifications of the shape of the blade-row loss buckets are the optimization design variables since they directly impact compressor performance and dynamic stability.

An optimization framework is defined, with the goal to redesign a baseline compressor through geometric modifications, optimized for enhanced stability. The framework is comprised of a mean line calculation including end-wall effects, and the computation of the unsteady flow field perturbations using the existing dynamic compression system model. A solution to the resulting inverse-blade-design problem introduced by the optimization problem is devised. Changes in blade-row loss buckets are linked analytically to a modification of the blade channel angle.

The inverse-design optimization framework is implemented on a 3-repeating-stage compressor leading to a 6.4% improvement of the stall margin while changes in performance are kept to a minimum of 2% loss in pressure ratio and 0.5% loss in efficiency. The definition of a new compressor geometry is obtained from the baseline compressor through the introduction of modifications to the blade channel angles of the blade-rows which range between -0.3° and 2.7°.

Thesis Supervisor: Professor Zoltán Spakovszky
Title: C.R. Soderberg Assistant Professor of Aeronautics and Astronautics

Acknowledgements

I first want to thank Professor Spakovszky for all the fruitful discussions that we had over the year. I am thankful for his support, his always critical look at my work leading to deeper understanding and better outcomes.

I am also grateful to my research partner Josep M. Dorca-Luque for the great moments we spent working together during which he shared with me his experience in the turbo-machinery world. Beyond work, we developed a real friendship and I must acknowledge that he taught me how to talk to computers in Catalan.

I am indebted to my officemates Chris, David and Mark for teaching me each day new things about this country and who took a real part in my introduction to the true American Experience. I also want to thank Alexis, my lab mate and social hour co-organizer, for the always enjoyable moments spent talking together.

My last thanks go to Professor Carrère from my engineering school ENSAE in France, for being one of the instigators of the joint project with MIT and who enabled me to enjoy this wonderful time spent here at the Gas Turbine Lab.

Contents

List of Figures

List of Tables

Nomenclature

roman

B	transmission matrix
c	polynomial interpolation coefficients
CFD	Computational Fluid Dynamics
DF	Diffusion Factor
EC	exit conditions
ECL	Ecole Centrale Lyon
ENSAE	Ecole Nationale Supérieure de lAéronautique et de l'Espace
f	function linking blade-row loss and geometry
g	blade staggered spacing
g	inequality constraint
GA	Genetic Algorithm
h	equality constraint
i	incidence, index
IC	initial conditions
j	$j = \sqrt{-1}$
J	objective function
k	correlation coefficient
L	blade-row loss coefficient
m	correlation coefficient
M	Mach number
$\dot{m}$	mass flow
n	correlation coefficient, harmonic number
OPR	Overall Pressure Ratio
P	pressure
P_t	total pressure
R	stage reaction
Re	Reynolds number
s	Laplace variable
S	search direction
SM	Stall Margin
SQP	Sequential Quadratic Programming

$\mathbf{T}$	transmission matrix
U	mean wheel speed
v	tangential velocity
V	non dimensional absolute velocity, relative velocity
$\mathbf{x}$	design vector
$\mathbf{X}$	transmission matrix
$\mathbf{Y}$	transmission matrix

greek

α	absolute flow angle, distance from previous point
β	relative flow angle
δ^*	end-wall axial-velocity boudary layer displacement thickness
Δ	difference (when used as a prefix)
Δ_{bc}	blade channel angle modification
ϕ	flow coefficient
γ	blade stagger angle
η	adiabatic efficiency
λ	blade-row inertia, interpolation coefficient, Lagrange multiplier, objective weight
μ	stator blade-row inertia
ξ	interpolation coefficient
ρ	fluid density
σ	growth rate / rotor frequency
τ	time lag
υ	end-wall tangential-force boundary layer thickness
Ψ	pressure rise
ω	blade-row loss coefficient
ω	rotation rate / rotor frequency

subscripts

1	inlet or upstream
2	outlet or downstream
ax	axial
design	at design point
gap	inter-blade-row gap
h	hub

peak	at the peak
R	rotor
ref	reference
rot	rotor
S	stator
sta	stator
stall	at stall point
sys	system
θ	circumferential direction
t	tip
x	cartesian coordinate
z	cartesian coordinate

supercripts

is	isentropic
ts	total-to-static

Chapter 1

Introduction

Currently, a number of research efforts focus on the optimization of the geometry of compressor blade-rows. For instance, Büche et al. [2] focus on the optimization of single subsonic compressor rows for aerodynamic performance (operating range and loss level) and mechanical integrity. As reflected in [2], the industry-practice main objective for compressor optimization is aerodynamic performance. In industry, compressors are designed for enhanced performance while stability requirements are introduced as constraints, but not prime design variables. This research features a new approach: a compressor design optimization framework *for enhanced stability* is established, based on dynamic compression system modeling. The overall stability of a compressor, in the light of its performance, is to be optimized. The inclusion of stability as a new design objective re-shapes the design space boundaries and thus opens regions never explored before, leading to new possibilities and enabling more aggressive designs. Such an approach could help engine manufacturers develop more robust engines (i.e. more resistant to transient operation, inlet distortion, icing, engine deterioration, etc.) at low cost, since stability problems encountered, once the engine is designed, can lead to costly modifications. These costly modifications could be avoided by design optimizations for enhanced stability.

This chapter first outlines some theoretical principles regarding rotating stall and surge mechanisms, then presents the motivations of this thesis with the objectives and contributions.

1.1 Technical Background: Rotating Stall and Surge

Rotating stall and surge in axial compressors have been the subject of numerous academic theses, research articles or technical books for many years. This indicates the importance attached to the understanding of the physical mechanisms leading to rotating stall and surge in order to prevent them from occurring in-flight. It is hence useful to review succinctly the stall and surge inception mechanisms (for more details, refer to Cumpsty [3], Greitzer [6] and Longley [10]).

Rotating stall is a localized phenomenon in which regions of stalled flow (referred to as stall cells) appear over a sector of the circumference of a compressor. This is basically a way for the compressor to adapt to small mass flows. Some regions contain locally high mass flows. Others contain almost no flow at all: these are the stalled regions. These regions of stalled flow travel circumferentially at a fraction of the compressor rotation rate, at frequencies between 20-50 % of rotation speed.

Surge is, on the other hand, a compression-system instability. The annulus averaged mass flow and the system pressure rise during surge undergo large amplitude oscillations. The frequencies of these oscillations are generally at least one order of magnitude below those associated with passage of a rotating stall cell and depend on the parameters of the entire system. In addition, during the surge cycles, the instantaneous mass flow through the compressor changes from values at which (in steady operation) the compressor would be free from stall, to values at which one would find rotating stall or totally reversed flow.

Both of these phenomena (surge and rotating stall) are seen to be quite distinct. However, they are not unrelated, since often the occurrence of the local instability (associated with the onset of rotating stall) can trigger the more global type of instability (leading to surge). Reducing the mass flow from the operating point, a maximum pressure ratio is achieved as shown in Figure 1-1. Beyond this point, the compressor enters into either stall or surge. The point of occurrence of this phenomenon is referred to as the stall point.

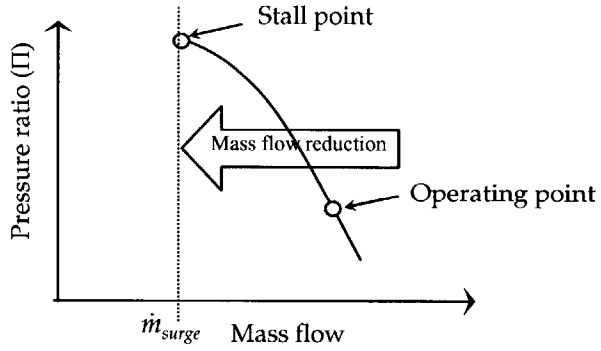

Figure 1-1: Pressure ratio – Mass flow characteristic showing the location of the stall point.

Stall Inception Mechanisms

The basic explanation of the mechanism associated with the onset of stall propagation can be summarized as follows (described by Greitzer in [6]). Consider a row of axial compressor blades operating at a high angle of attack, such as shown in Figure 1-2. Suppose that there is a nonuniformity in the inlet flow such that a locally higher angle of attack is established near blade B which is enough

to stall it. If this happens, the flow can separate from the suction surface of the blade so that a substantial flow blockage occurs in the channel between B and C. This blockage causes a diversion of the inlet flow away from blade B and towards C and A (as shown by the arrows), resulting in an increased angle of attack on blade C and a reduced angle of attack on blade A. Since C was on the verge of stall before, it will now tend to stall, whereas the reduced angle of attack on A will inhibit its tendencies to stall. The stall will thus propagate along the blade-row in the direction shown, and under suitable conditions it can grow to a fully developed cell covering half the flow annulus or more. When covering a wide circumferential sector of the annulus and extending over the full length of the machine, the flow disturbances are referred to as *modal oscillations*. The term "modal" defines circumferential modes, the first mode having a wavelength equal to the circumference, the second twice its circumference, etc. (see Figure 1-3) .

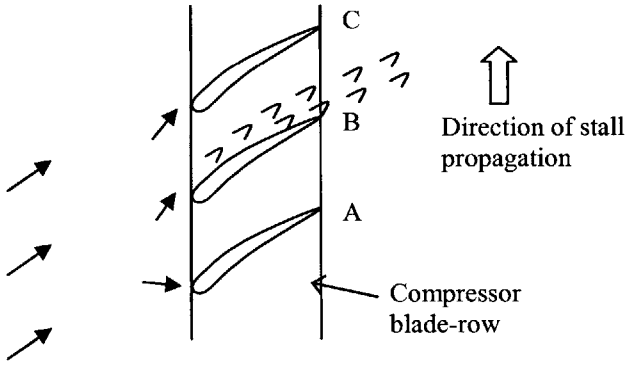

Figure 1-2: Physical mechanism for inception of rotating stall (from [6]).

It has to be kept in mind that rotating stall and surge are the mature forms of small amplitude flow perturbations that are the natural resonances of oscillations in the compression system, these small disturbances grow when background flow conditions are such that their damping becomes negative and the compression system drops into an unstable state, rotating stall or surge.

Spakovszky (see [15] and [16]) developed an analytical, dynamic compression system model aimed at the determination of the fundamental flow resonances (circumferential modes or eigenvalues of the unsteady flow field) in axial and radial compressors. Spakovszky's dynamic compression system model is the central part of this thesis, and is used to predict the stability of axial compressors. The model will be presented with more detail in Chapter 2.

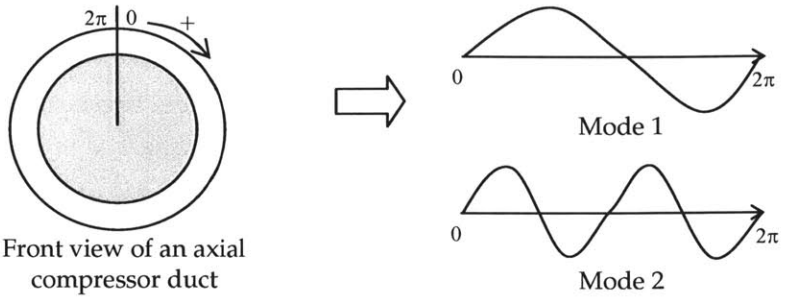

Figure 1-3: Schematic presenting the circumferential modes.

Stability Analysis of a Compression System

Two criteria have to be met for a compression system to be stable: static stability and dynamic stability. Static instability (illustrated on the left of Figure 1-4) is associated with a pure divergence from initial state (analogous to a mechanical system with negative spring constant) and is related to the slopes of the throttle line and the compressor characteristic. For a small perturbation in mass flow (a decrease, say), if the system is operating at point A, a pressure imbalance will arise to cause fluid accelerations that return the system to operation at the initial point. Point A is thus a stable operating point. At point B, however, where the throttle line is tangent to the compressor characteristic, the pressure forces associated with a small decrease in mass flow will cause the system to depart further from the initial operating point, so that point B is an unstable operating point.

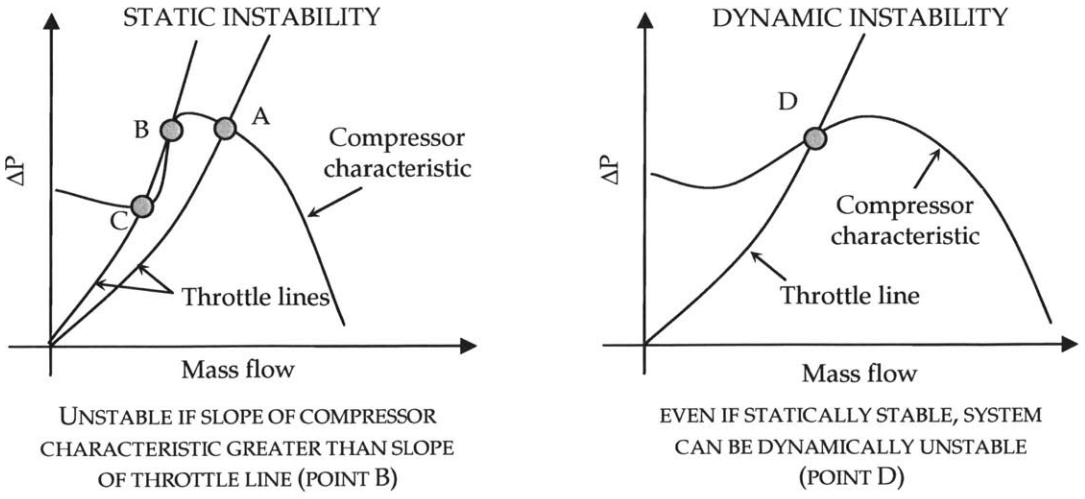

Figure 1-4: Types of compression system instability (adapted from [7]).

This first criterion is, however, too simple to describe the real phenomenon, since it only considers the static stability of the system. In fact, it is generally the dynamic stability criteria which are violated first, leading to growing oscillatory motion. As indicated on the right side of Figure 1-4, a compression system can be statically stable (according to the foregoing slope criterion) and still exhibit instability. In summary, static stability is necessary for a compression system to be stable but is not sufficient.

The static and dynamic stability behavior of compression systems is captured by Spakovszky's dynamic model.

1.2 Why Design for Enhanced Stability?

Why should stability be taken into account at the early stage of compressor design?

Blanvillain [1] assessed how much an in-flight surge event potentially costs an airline operating such an aircraft. This type of problem is a very unwanted event because it can cost the airline up to $3.5 million. Furthermore, running a fleet of reduced-stability engines can cost a major airline up to $10 million a year. These expenses can represent up to 8% of the total revenue potentially generated by the fleet powered by these engines. The probability of in-flight surge could be reduced and engine stability enhanced if stability was taken into account from the early stage of design.

Furthermore, to limit potential risks associated with surge events, industry design practice and certification authorities impose a substantial margin, called stall margin (or surge margin), intended to keep the engine operating away from the stall boundary. Several uncertainties are associated with stall margin, such as inlet distortion, transient operation, icing or engine deterioration. All these uncertainties are built into stall margin that is consequently increased, leading to a reduction in blade loading and diffusion, entailing sub-optimal designs as operating conditions are typically moved away from points of high efficiency. The key idea of this research is to incorporate dynamic stability as a prime design objective and to establish a compressor design framework optimizing for enhanced stability.

First, the background and motivation for this thesis are introduced followed by the presentation of a joint project in which this research is embedded.

1.3 The Joint Project

This thesis is part of a joint project initiated in 2001 by Snecma Moteurs, the Ecole Nationale Supérieure de l'Aéronautique et de l'Espace (ENSAE), the Ecole Centrale de Lyon (ECL) and the Massachusetts Institute of Technology. This project is aimed at educating future engineers by giving

them an opportunity to work in an international environment on complex systems and to develop their skills in the gas turbine engine field. A detailed description of the respective contributions of the parties involved is reviewed in Blanvillain [1].

MIT's part of the project focuses on the inverse-design of an axial compressor using an existing reduced order dynamic compressor model embedded in an optimization framework for performance and stability.

The architecture of this framework is presented in Figure 1-5. From an original aerodynamic design, performance characteristics of a compressor can be obtained and its dynamic behavior can be evaluated using the reduced order model. Once the dynamics of the modal oscillations are determined, a metric is involved to assess the dynamic stability of the system. The shape of the loss buckets can then be altered in an inner optimization loop in order to increase the level of stability to pre-defined objectives. The shapes of the loss buckets are chosen to be the optimization design variables since compressor stability is affected by the loss characteristics. This is because the compression system dynamics consist of pre-stall modes which depend on the background flow field.

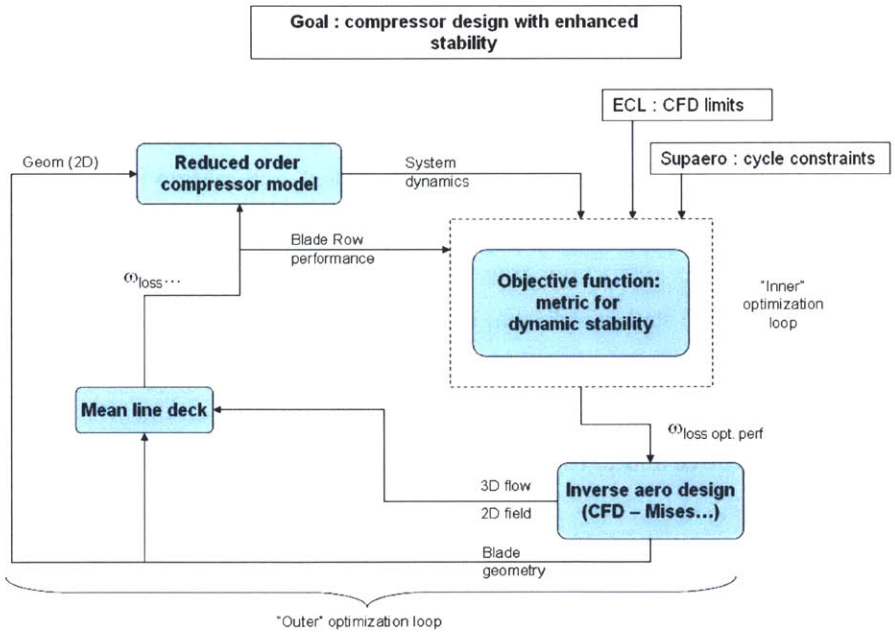

Figure 1-5: Joint project framework.

The last task is the definition of the geometric modifications leading to the prescribed loss buckets. This inverse-design problem can be solved using CFD calculations and a mean line deck. The new geometry obtained from the prescribed loss buckets is then fed into the dynamic calculation and the process is repeated until convergence in performance and stability is achieved.

1.4 Previous Work and Ongoing Efforts

This thesis is the second step of the project. Blanvillain's work represented the first-year effort. He implemented Spakovszky's reduced order model [15] for a multi-stage axial compressor, and carried out a series of parametric studies aimed at defining preliminary compressor design guidelines for enhanced stability.

The project was then divided into two parallel efforts. This thesis focuses on the inverse-design optimization for enhanced stability. A more thorough description of the optimization framework is given in next section. The other effort carried out at the same time by Dorca [4] focuses on an energy-based analysis of compressor stability and is aimed at the development of a metric for stability that could eventually be used as an optimization objective.

1.5 Thesis Organization

The optimization framework developed in this thesis is now presented. It is an implementation of the inverse-design architecture presented in section 1.3, although it differs from it since the inverse design optimization for enhanced stability is solved in a single optimization loop.

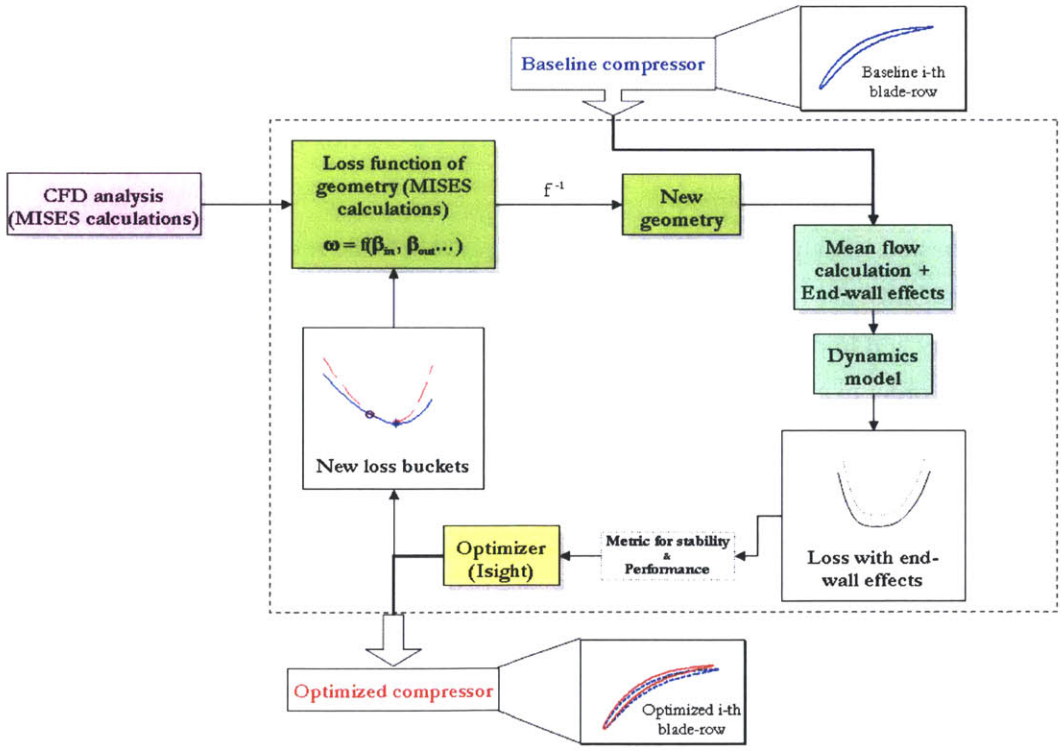

Figure 1-6: Diagram presenting the optimization framework.

Figure 1-6 depicts the path followed from a given baseline compressor to the eventual optimized compressor for enhanced stability. The main idea as follows: a baseline compressor to be optimized for stability is defined in terms of its geometry and individual blade-row losses. The performance of the baseline compressor is computed using a mean line calculation including end-wall effects and the eigenvalues for modal flow oscillations are found using Spakovszky's model (performance and dynamic calculations are described in Chapter 2). From the aforementioned calculations, the level of performance and stability of the baseline compressor are measured.

The loss buckets of the blade-rows are then modified by using the commercially available optimizer Isight, with the objective of achieving a prescribed level of stability in the light of performance constraints. The shapes of the blade-row loss buckets prescribed by the optimizer are then linked to geometric modifications inside the optimization loop. The steps (based on a preliminary CFD analysis) leading to the determination of a function f, the solution to the inverse-design problem linking a change in a blade-row loss bucket to a modification of a blade-row geometry, are described in Chapters 3, 4 and 5.

Once the new geometry stemming from the new loss buckets is defined, the calculation is iterated until an optimized solution meeting the stability and performance requirements is found. The optimization process is explained in Chapter 6 leading to the optimization of a 3-stage repeating-stage compressor.

1.6 Objectives

The objectives of this thesis are to:

- Assess and analytically describe the relation between blade-row loss, geometry, performance and stability.
- Identify and implement geometric design variables linked to modifications of the blade-row loss in order to perform a compressor design optimization for enhanced stability.
- Propose a design framework capable of optimizing a compressor for enhanced stability in the light of performance constraints, using an existing dynamic compressor model.
- Demonstrate the framework capabilities by solving an optimization problem for a generic 3-stage, repeating-stage compressor comprised of blade-rows with NACA0012 profiles.
- Devise design implications using the optimization framework.

1.7 Contributions

The contributions of this thesis can be summarized as follows:

- Definition of an inverse-design optimization framework for enhanced compressor stability, based on dynamic compression system modeling,
- Feasibility assessment of the compressor design framework optimizing for enhanced stability,
- Implementation and demonstration of this design-framework for a 3-repeating-stage compressor.

Chapter 2

The Optimization Loop: Major Features

To perform the optimization loop as presented in Figure 1-6 going from a baseline compressor to the optimized one, a simulation code or optimization loop is needed to implement and to combine the mean line calculation, the dynamic model, the loss interpolations and the end-wall correlations. This loop will eventually be closed by the optimizer which enables the iterative optimization process. Without going into the details of the optimization, this chapter focuses on all the components that have to be combined to form the optimization framework. The aim is the following: a compressor geometry is specified, given the losses and deviations corresponding to each blade-row, and the operating conditions (speed, external thermodynamic conditions). From this set of data, one wants to be able to predict:

- the compressor ***performance*** (typically overall pressure ratio and overall adiabatic efficiency) computed using a compressible mean flow calculation including end-wall effects and taking into account deviation and loss data. Performance is to be computed at low speed because Mach number effects on the losses and additional shock-induced losses are neglected.
- the compressor ***stability*** (taking for instance stall margin as a metric for stability) computed using an incompressible compression system dynamic model.

Keeping these objectives in mind, this chapter first introduces an overview of the different steps encountered in the optimization loop. Next, all the linked modules are presented along with their limitations and the assumptions made.

2.1 Overview of the Optimization Loop

Before describing all the modules, an overview of the framework is given, together with the links between the different components. Figure 2-1 presents a sketch of the loop that is eventually closed by the optimizer.

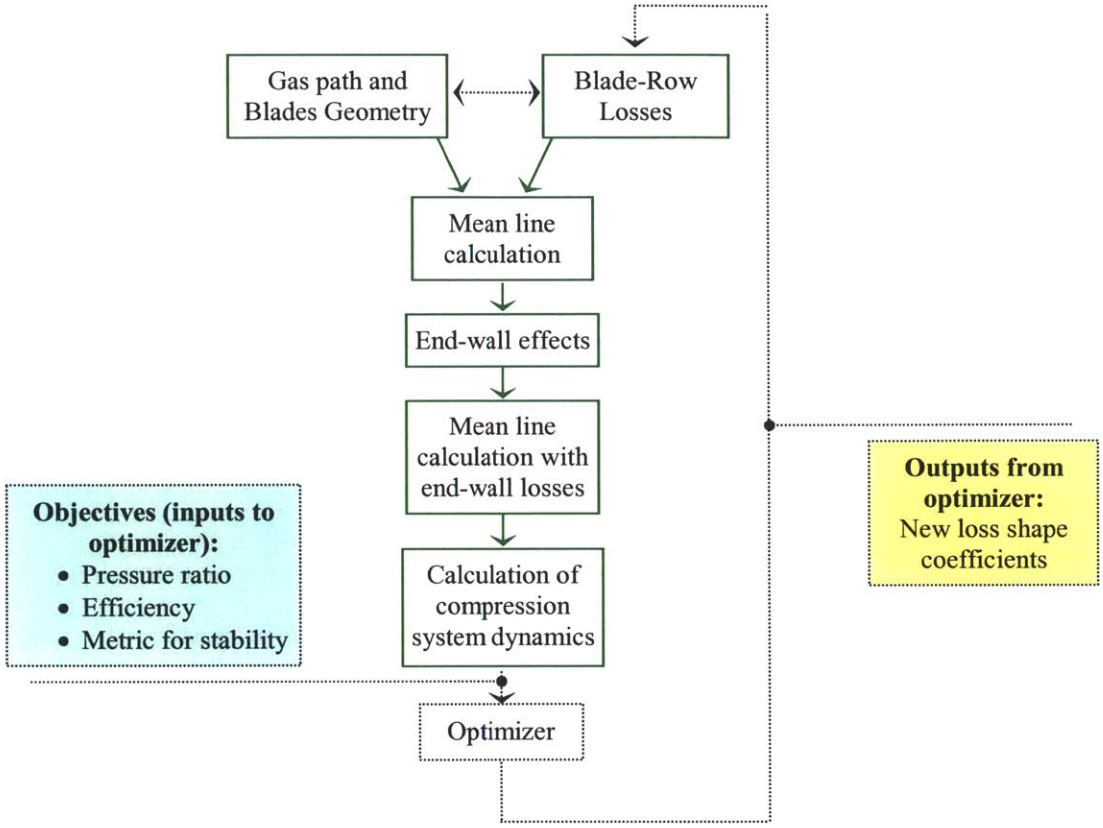

Figure 2-1: Overview of the optimization loop.

Conceptually, the aim of the optimization loop is to compute the overall pressure ratio, adiabatic efficiency and stall margin of a given compressor.

The inputs to the calculation are the geometry of the gas path and the blades, as well as the loss descriptions of all the blade-rows. To get the compressor performance, a first mean line calculation using these inputs is performed. From this performance, end-wall correlations are implemented, leading to a re-definition of the blade-row loss, including end-wall effects.

The mean line calculation is then performed for the second time using the loss buckets with end-wall effects as inputs. This mean line calculation also provides the velocity field, flow angles, blade-row loss and loss derivatives, which are necessary inputs to the calculation of the compressor pre-

stall dynamics. This calculation enables the computation of the compressor stall margin which is another objective function in the optimization loop.

Next, more details on the mean line calculation, the dynamic compressor model, and the implementation of end-wall effects are given.

2.2 Mean-Line Calculation

The mean line calculation is used to compute the performance of any given compressor (one is interested in the overall pressure ratio and the overall adiabatic efficiency). For that calculation to be carried out, the following inputs have to be specified:

- number of stages,
- hub and tip radii at mid-axial position between each blade-row,
- lengths of the blade-row and inter-stage gaps,
- blade chords,
- inlet and outlet metal angles as well as stagger angles for all blade-rows.

Furthermore, the inlet flow conditions and rotational speed have to be specified:

- inlet static pressure and temperature,
- rotation speed,
- inlet swirl angle.

Finally, the effects of blade-row loss and deviation (functions of incidence) have to be input.

Using this data, the compressor performance is obtained, that is the overall pressure ratio and the overall adiabatic efficiency maps as functions of corrected mass flow.

The mean line calculation used in this research makes the following assumptions:

- A 1D pitchline calculation is performed at the mean radius (mean radius computed using Euler's definition).
- The calculation is compressible, implying that an iterative solution procedure is needed to define the axial velocity along the compressor. However, losses are assumed to be only function of incidence: Mach number effects are assumed to be negligible. This assumption is valid if the blades are thin and have small camber, and if the relative Mach

numbers stay below 0.7, value above which Mach number effects on loss become significant.

A more detailed description of this mean line calculation is given in Appendix A.

2.3 Reduced Order Dynamic Compressor Model

2.3.1 Underlying Theory

The other goal of the optimization loop apart from computing performance is to predict compressor stability. Spakovszky [15] developed a dynamic compression system model well-suited for the stability prediction of any axial compressor. This compression system model is implemented in this research and a brief description of the major features is given in this section. For more details and the derivation, see [15].

The idea of the dynamic compressor model is to examine the behavior of unsteady, small amplitude perturbations to a known steady-state flow field. For that purpose, each of the flow field quantities is decomposed into a steady component and an unsteady, small amplitude perturbation. The unsteady perturbations are then decomposed into their circumferential spatial harmonics. The behavior of these spatial harmonics is computed and the system stability is determined by analyzing the resulting eigenvalues or system modes.

A modular approach is adopted and casts each system component (rotor, stator, gap or duct) into a transmission matrix that can be linked to any other system component by simply stacking the matrices.

The model is illustrated in an example implementation for a single-stage axial compressor as shown in Figure 2-2.

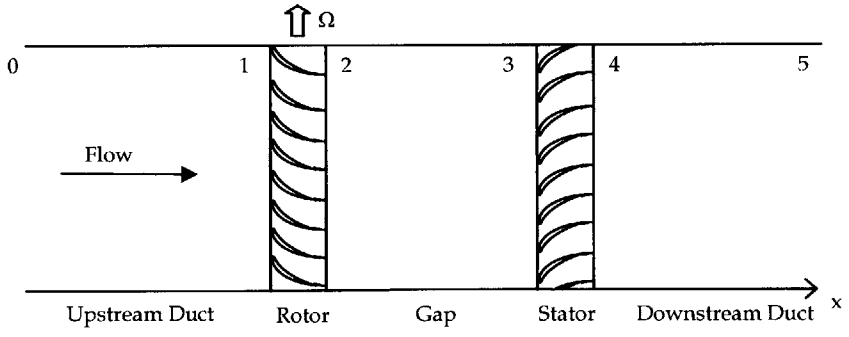

Figure 2-2: Single-stage axial compressor model.

The eigenvalues of the modeled compression system are given by the solution of the eigenvalue problem presented in equation (2-1), for each spatial harmonic number n. The solution of this equation is non-trivial since both the eigenvalues and the function $\mathbf{Y}_{sys,n}$ are complex:

$$\det\{\mathbf{Y}_{sys,n}(s)\}=0 \quad \forall n \succ 0 \tag{2-1}$$

$$\text{with } \mathbf{Y}_{sys,n}(s)=\begin{bmatrix} EC\cdot\mathbf{X}_{sys.n}(s) \\ IC \end{bmatrix} \tag{2-2}$$

$$IC=\begin{bmatrix}0 & 1 & 0\\ 0 & 0 & 1\end{bmatrix}, EC=\begin{bmatrix}1 & 0 & 0\end{bmatrix} \text{ (boundary conditions),}$$

$$\text{and where } \mathbf{X}_{sys.n}(s)=\mathbf{T}_{ax,n}(x_4,s)^{-1}\cdot\mathbf{B}_{sta,n}(s)\cdot\mathbf{B}_{gap,n}(s)\cdot\mathbf{B}_{rot,n}(s)\cdot\mathbf{T}_{ax,n}(x_1,s). \tag{2-3}$$

The eigenvalues $s=\sigma-j\omega$ of the modeled compression system are solutions of equation (2-1). σ_n is the growth rate and indicates whether the perturbation wave amplitude grows in time, leading to an unstable system (positive growth rate), or decays in time, leading to a stable system (negative growth rate). ω_n is the rotation rate of the n^{th} spatial harmonic perturbation.

Furthermore, in equation (2-2), $\mathbf{X}_{sys.n}$ contains all the stacked matrices modeling each system component as described in equation (2-3).

$\mathbf{T}_{ax,n}$ is the transmission matrix for an axial duct, defined as:

$$\mathbf{T}_{ax,n}=\begin{bmatrix} e^{nx} & e^{-nx} & e^{-\left(\frac{s}{\overline{V_x}}+jn\frac{\overline{V_\theta}}{\overline{V_x}}\right)x} \\ je^{nx} & -je^{-nx} & \left(-\frac{sj}{\overline{V_x}n}+\frac{\overline{V_\theta}}{\overline{V_x}}\right)e^{-\left(\frac{s}{\overline{V_x}}+jn\frac{\overline{V_\theta}}{\overline{V_x}}\right)x} \\ \left(-\frac{s}{n}-\overline{V_x}-j\overline{V_\theta}\right)e^{nx} & \left(\frac{s}{n}-\overline{V_x}+j\overline{V_\theta}\right)e^{-nx} & 0 \end{bmatrix} e^{jn\theta};$$

$\mathbf{B}_{rot,n}$ is the transmission matrix for a rotor:

$$\mathbf{B}_{rot,n} = \begin{bmatrix} 1 & 0 & 0 \\ \tan\beta_2 & 0 & 0 \\ \left[\tan\beta_2 - \lambda_r(s+jn) + \dfrac{\partial L_R}{\partial \tan\beta_1}\dfrac{\tan\beta_1}{\overline{V_x}(1+\tau_R(s+jn))} - \overline{V_{\theta 2}}\tan\beta_2\right] & -\dfrac{\partial L_R}{\partial \tan\beta_1}\dfrac{1}{\overline{V_x}(1+\tau_R(s+jn))} + \overline{V_{\theta 1}} - 1 & 1 \end{bmatrix} e^{jn\theta};$$

$\mathbf{B}_{sta,n}$ is the transmission matrix for a stator:

$$\mathbf{B}_{sta,n} = \begin{bmatrix} 1 & 0 & 0 \\ \tan\alpha_2 & 0 & 0 \\ \left[-\lambda_s s + \dfrac{\partial L_S}{\partial \tan\alpha_1}\dfrac{\tan\alpha_1}{\overline{V_x}(1+\tau_S s)} - \overline{V_{\theta 2}}\tan\alpha_2\right] & -\dfrac{\partial L_S}{\partial \tan\alpha_1}\dfrac{1}{\overline{V_x}(1+\tau_S s)} + \overline{V_{\theta 1}} & 1 \end{bmatrix} e^{jn\theta};$$

and finally, $\mathbf{B}_{gap,n} = \mathbf{T}_{ax,n}(x_3, s)\cdot\mathbf{T}_{ax,n}(x_2, s)^{-1}$.

After this brief presentation of the model, its implementation is presented in order to determine the level of stability of a given axial compressor.

2.3.2 Eigenvalue Search to Determine the Point of Limit Stability

The solution of equation (2-1) provides a set of eigenvalues corresponding to different modes and harmonics (Figure 2-3 depicts the example of a 3-stage compressor, the eigenvalues of five strings of modes are represented, four harmonics per string).

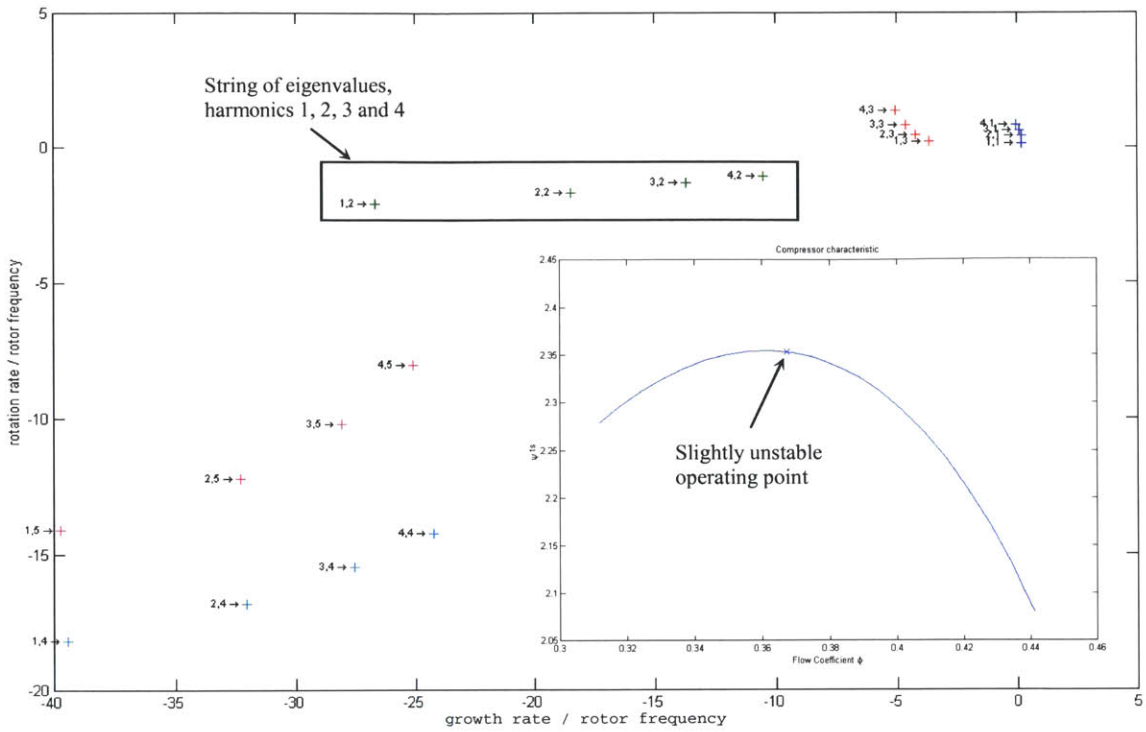

Figure 2-3: Eigenvalues for a 3-stage compressor for a given operating point shown on the corresponding compressor characteristic.

The stall point occurs when the growth rate (σ) of the least stable eigenvalue becomes positive. Hence, one can focus on the real part of that particular eigenvalue in order to determine stability:

$$\sigma > 0 : \text{unstable compressor},$$
$$\sigma < 0 : \text{stable compressor}.$$

As shown in Figure 2-3 for an unstable compressor, only one string of modes (the one with non-dimensional growth rate near 0) is of interest near the stall point, as all other strings of modes are well damped (non-dimensional growth rate lower than -3).

Using the eigenvalue properties above, a method to sweep the compressor characteristic is needed until the point of limit stability is found. Such a method was developed and is illustrated in Figure 2-4, sketching the iterative process as a function of the compressor mass flow. A detailed description of this process is given below.

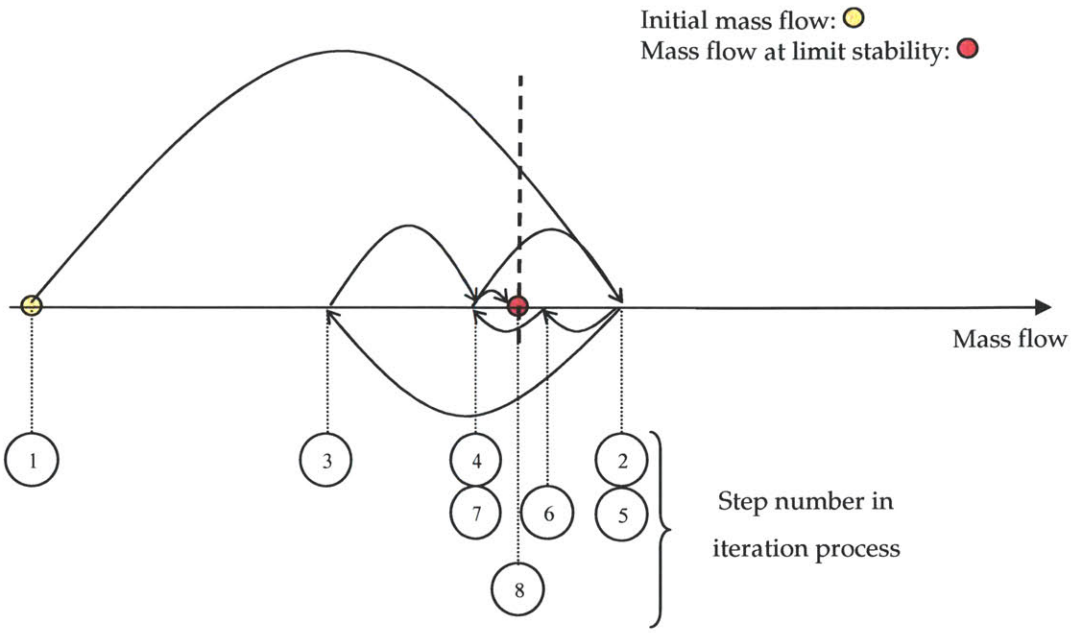

Figure 2-4: Schematic of the search routine to determine the point of limit stability.

The principle is the following: an initial mass flow is given, at which the compression system dynamics are determined, and the eigenvalue belonging to the least stable mode, usually the first harmonic, is found. Depending on the sign of the real part of the eigenvalue (σ), that is depending on the system stability, the mass flow is increased or decreased to get closer to the point of limit stability. As soon as σ changes sign, meaning that the compression system switched from an unstable configuration to a stable configuration (or vice versa), the step in mass flow is reduced, and the iteration process carries on until the point of limit stability is found.

In the calculation procedure, the following parameters need to be defined:

- initial mass flow
- step in mass flow
- tolerance (convergence criterion)

These parameters can be adjusted, depending on the type of compressor, in order to improve the speed of convergence.

2.4 End-Wall Correlations

To refine the mean line calculation and also to be potentially able to use a 3D calculation including end-wall effects as a check, a module computing end-wall losses is implemented. A version of the flow solver MISES extended by Lavainne [9], who implemented end-wall correlations in the calculation, is available. Hence, if one wants to compare the performance of the optimized compressor computed by the optimization loop to the one computed with MISES, end-wall effects on losses need to be implemented inside the optimization loop.

The correlations used are the ones presented by Smith, based on an experimental study of casing boundary layers in multistage axial-flow compressors [13]. The main ideas of these correlations are presented next.

The correlations are based on the hypothesis that the axial velocity distribution along a blade span inside a repeating-stage compressor can be divided into three regions: a free-stream region (modeled by the mean line calculation) and two end-wall-boundary-layer regions. Smith further shows that the end-wall boundary layer thicknesses depend primarily on three quantities: the blade-to-blade passage width, the aerodynamic loading level, and clearances. Correlations are set up to compute this information in order to be able to predict how the pressure-flow and efficiency-flow characteristics are modified by end-wall effects.

To determine the performance of a compressor-stage with end-wall effects, a three-step calculation method is performed:

- First, performance is computed for each stage using the mean line calculation (presented in section 2.2), ignoring end-wall effects (quantities obtained from this first calculation step are denoted by tilde (~)).
- Then the end-wall axial velocity boundary layer displacement thicknesses (δ^*) and end-wall tangential-force boundary layer thicknesses (v) at hub and tip are computed (the precise definition of these quantities can be found in [13]). The correlations presented by Smith [13] are used to obtain these quantities. They mainly depend on the blade staggered spacing (as defined in Figure 2-5), static pressure rise of the stages, maximum static pressure rise and tip clearance.
- Finally, the efficiency and flow coefficient are computed using the previously calculated quantities. The following formulas are used, as presented by Smith.

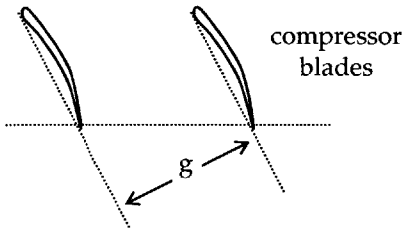

Figure 2-5: Definition of the blades staggered spacing (g).

For high hub/tip ratio stages, the efficiency with end-wall effects can be approximated by

$$\eta = \tilde{\eta}\frac{1-\dfrac{\delta_h^* + \delta_t^*}{h}}{1-\dfrac{\upsilon_h^* + \upsilon_t^*}{h}}. \tag{2-4}$$

Similarly, from the flow coefficient computed for the compressor without end-wall effects, the actual flow coefficient can be correlated using the following approximate formula

$$\varphi = \tilde{\varphi}\left[1-\left(\frac{\delta_h^*}{g_t}+\frac{\delta_t^*}{g_h}\right)\frac{\bar{g}}{h}\right]. \tag{2-5}$$

From the efficiencies and flow coefficients including end-wall effects, it is possible to get the pressure rise across each of the stages. The efficiency and pressure rise obtained from the calculation without end-wall effects are used to compute the isentropic pressure rise (using, the definition of efficiency: $\eta = \psi/\psi_{isentropic}$). Then, using the isentropic pressure rise and the efficiency calculated with equation (2-4), the definition of the efficiency is used a second time to get the pressure rise with end-wall effects. A flow coefficient shift is finally applied using equation (2-5), yielding the new pressure rise / flow coefficient characteristic. The procedure adopted is sketched next, followed by the explanation of the blade-row loss definition.

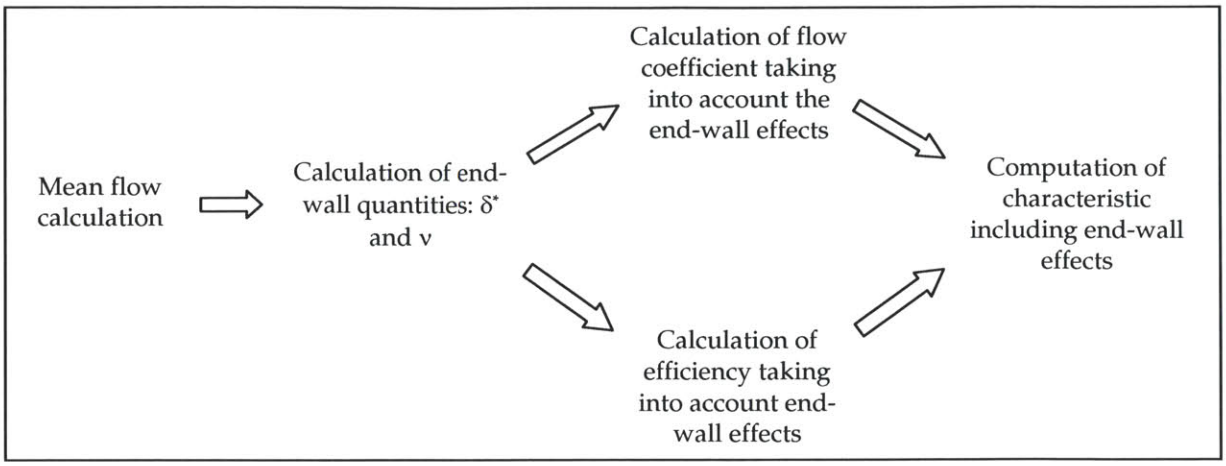

Figure 2-6: Calculation procedure implementing end-wall effects.

After performing this analysis, one wants to redefine the loss buckets adding the end-wall effects to the originally defined losses. To do so, the definition of the loss coefficient L as used in the dynamic compressor model is:

$$L = \frac{P_{t\ in}^{is} - P_{t\ out}}{\rho U^2}. \tag{2-6}$$

It is possible to compute individual stage loss with end-wall effects using the overall additional blade-row loss due to end-wall effects obtained from the compressor characteristic as shown in Figure 2-7.

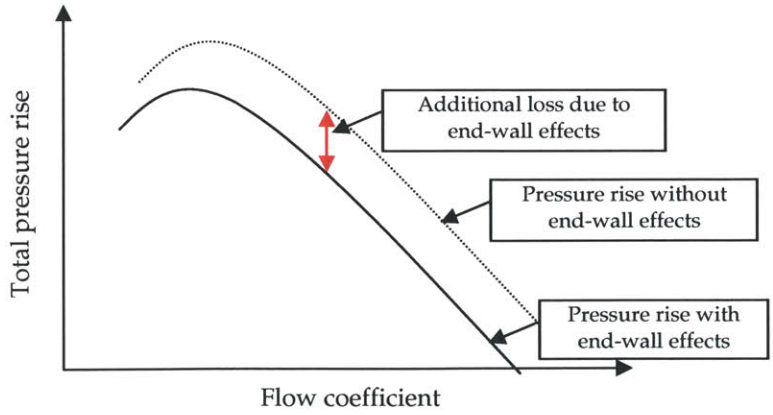

Figure 2-7: Additional stagnation pressure loss due to end-wall effects.

The computation of the stage stagnation pressure loss from the overall stagnation pressure loss is obtained by splitting the losses in as many stages as the compressor has. This assumes that the compressor has repeating stages, meaning that the flow pattern is similar in all the stages, hence that the overall additional loss due to end-wall effects can be divided into as many equal parts as there are stages. Then, to compute the blade-row losses from the stages loss, the stage reactions are used

$$L_{rotor} = L_{stage} \cdot R, \tag{2-7}$$

$$L_{stator} = L_{stage} \cdot (1 - R). \tag{2-8}$$

Limitations

It has to be kept in mind that the data used to determine the losses due to end-wall effects is limited. Smith [13] reports considerable scatter in the tangential force thickness of hub and casing boundary layers obtained from experimental data. As a consequence, numerical values can be taken within a certain uncertainty range, leading to uncertainties of the performance and stability calculations estimated to 4%.

Furthermore, the data given for the determination of the peak pressure rise coefficient is limited to:

- a Reynolds number of 200,000
- aspect ratios ranging from 2 to 5
- axial gap spacing non-dimensionalized by blade spacing (or pitch), ranging from 0.2 to 0.6
- multistage compressors made up of repeating stages

This means that the results obtained from these correlations are not applicable to compressors with any geometry. Other correlations will have to be applied to include Reynolds number effects and axial gap spacing effects. Concerning the aspect ratio, Smith [14] reports that the applicability of the method to low aspect ratio compressors is of particular concern, and that additional experimental data would be needed to justify the use of the same correlations for these types of low aspect ratio compressors.

Implementation

This section presents results obtained by the mean line calculation with and without end-wall effects. These two different sets of results are compared in Table 2-1 in order to check the relevance of the end-wall effects implementation. Calculations were performed on the 3-stage, repeating stage

compressor (the geometry of this compressor is presented in Appendix B, this particular compressor is used throughout the thesis and is optimized for enhanced stability in Chapter 6).

	Overall Pressure Ratio	Overall adiabatic efficiency
Calculation without end-wall effects	1.349	0.936
Calculation including end-wall effects	1.317	0.924

Table 2-1: Comparison of the 3-stage repeating-stage compressor performance with and without end-wall effects.

Both efficiency and overall pressure ratio follow the expected trend, with a decrease of 2.4% and 1.3% respectively due to losses stemming from end-wall effects.

Note that the level of adiabatic efficiency is high. This is because the secondary loss, that accounts for about 4% of the total loss in a compressor (as will be shown in Figure 3-1), is not taken into account in the calculations. That additional source of loss would yield more realistic values of the adiabatic efficiency, close to 0.88.

Finally, Figure 2-8 presents the losses before and after the end-wall effects are added. These two loss buckets are displayed here to show that the results obtained are reasonable. Although data available comparing blade-row loss buckets with and without end-wall effects are limited, a comparison was done with numerical calculations implementing end-wall effects for similar configurations (for more details, refer to Lavainne [9]). The loss variation due to end-wall effects is of the same order of magnitude in the numerical calculations and in the computations performed with the framework implemented in this thesis.

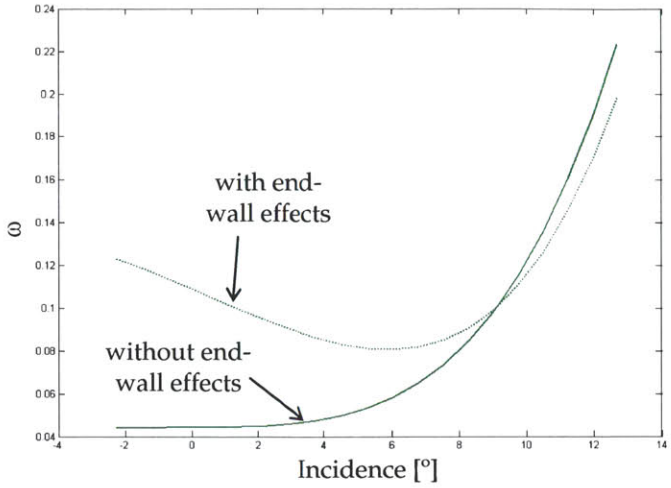

Figure 2-8: Loss bucket for rotor 1 of the 3-stage, repeating-stage compressor with and without end-wall correlations.

2.5 Conclusion

This chapter presented the optimization loop. All modules necessary to conduct the performance and stability calculations are defined, together with their limitations and the assumptions made. It was seen how overall pressure ratio, overall adiabatic efficiency and stall margin can be computed from the input of the geometry and blade-row loss of a compressor, enabling the implementation of the optimization loop.

This tool is used in the next chapters where influence of loss on performance and stability are dissected. The eventual step will be the implementation of this tool for the optimization of the 3-repeating-stage compressor.

Chapter 3

Influence of Blade-Row Losses on Compressor Performance and Stability

The following two chapters aim at showing the process that was adopted to find a geometric modification of the blade-rows (linked to loss modifications) to be implemented in the optimization framework. This process starts with the exploration and description of the way the shape of a blade-row loss bucket influences compressor performance and stability. The first aim of this chapter is to review mechanisms leading to stagnation pressure loss in turbo-machinery. The second goal is to analytically relate compressor stability to blade-row performance using the Moore-Greitzer model [11]. The final aim is to demonstrate how each blade-row contributes to the compressor pre-stall dynamics using the existing dynamic compressor model [15].

3.1 Compressor Characteristics From First Principles

First, some basic definitions are reviewed in order to provide physical insight about blade-row losses and their impact on stability and performance of a given compressor.

Definition of Losses

The end result of losses in turbo-machinery is a rise in entropy and a reduction in stagnation pressure compared to the inlet value or to an ideal value.

The following definitions of the stagnation pressure loss are used:

- total pressure loss coefficient, non-dimensionalized by the blade-row inlet dynamic pressure:

$$\text{for compressible flow: } \omega = \frac{\Delta p_t}{p_{t1} - p_1} = \frac{p_{t1} - p_{t2}}{p_{t1} - p_1},$$

for incompressible flow: $\omega = \frac{p_{t1} - p_{t2}}{\frac{1}{2}\rho V^2}$.

- total pressure loss coefficient used in incompressible dynamic compressor model:

$$L = \frac{\Delta p_t}{\rho \mathbf{U}^2} = \frac{p_{t1} - p_{t2}}{\rho \mathbf{U}^2}.$$

Note that for incompressible flow, stagnation pressure loss is proportional to $1/2\,\rho V^2$ and is function of incidence (where incidence is a function of axial and circumferential velocities V_x and V_θ). If an IGV fixes the inlet flow angle into a compressor, small changes in V_x and V_θ are not independent. Thus, the flow coefficient ($\phi = V_x/\mathbf{U}$) effectively determines the incidence and hence the performance of a given compressor stage. For this reason, in incompressible flow, the loss as a function of incidence $\omega(i)$ is equivalent to the loss as a function of flow coefficient $L(\phi)$.

Several mechanisms lead to stagnation pressure loss in turbo-machinery. One possible breakdown of the overall loss is: profile loss, secondary loss and end-wall loss or annulus loss.

Profile loss is usually taken to be the loss generated in the blade boundary layers well away from the end-walls. The extra loss arising at a trailing edge due to the mixing process of the velocity non-uniformities is usually included as profile loss. Secondary loss arises from the secondary flows that develop in a compressor duct, lead to mixing processes and generate entropy. End-wall loss or annulus loss arises from the end-wall-boundary-layer regions of the blades.

Cumpsty ([3]) quotes the estimate for the different loss sources given by Howell (1945), shown here in Figure 3-1.

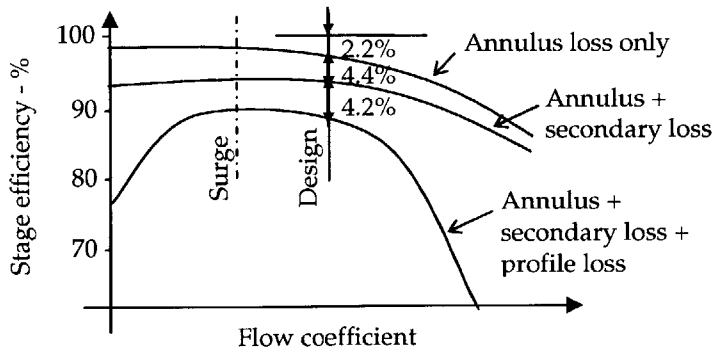

Figure 3-1: Howell's breakdown of loss for an axial stage (From Cumpsty [3]).

Compressor Characteristic

For the sake of transparency, the example of an incompressible one-stage compressor is taken. From Euler turbine equation, the isentropic total pressure rise across the stage can be written as:

$$\psi^{is} = 1 - \phi(\tan\beta_2 + \tan\alpha_1).$$

The angles in that formula are fixed primarily by the metal angles of the compressor, although they are not strictly constant since the flow undergoes some deviation at the blade-rows exit.

The single-stage compressor pressure rise is obtained from the isentropic pressure rise, subtracting stagnation pressure loss across the rotor (L_R) and across the stator (L_S)

$$\psi = \psi^{is} - L_R - L_S = \psi^{is} - L.$$

The following sketch depicts the influence of losses on the isentropic pressure rise leading to the single-stage compressor characteristic:

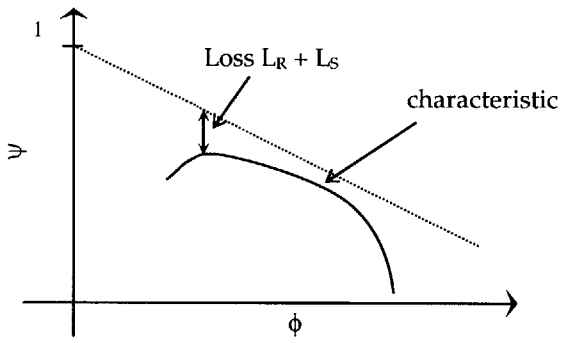

Figure 3-2: Sketch of a compressor characteristic.

Compressor Stability

Compressor stability is directly linked to the loss slopes $\partial L/\partial\phi$. The relation between loss and stability of a compression system was analytically formulated by Moore and Greitzer [11]. They modeled a compressor using the following assumptions: all blade-rows are lumped into a single semi-actuator disk, inlet and outlet ducts are infinitely long, and the effects of unsteady loss are neglected. The Moore-Greitzer model has the advantage of being analytically solvable, and the linearized solution to the eigenvalue problem yields for the n^{th} harmonic compressor mode $s = \sigma_n - j\cdot\omega_n$ where:

$$\sigma_n = \frac{\frac{\partial \psi^{ts}}{\partial \phi}}{\mu + \frac{2}{n}} \quad \text{and} \quad \omega_n = \frac{\lambda n}{\mu + \frac{2}{n}}.$$

λ is the blade passage fluid inertia of the rotors, and μ of the rotors and stators.

In this simplified case, the compression system is stable (negative growth rate s) for operating points with a negative slope of total-to-static pressure rise coefficient with respect to flow coefficient and unstable for a positive slope (positive growth rate). Although it is not always possible to analytically express the relation between compressor performance and stability like in Moore-Greitzer model, the modes of a compression system and the blade-row performance are always coupled. This is because the compression system dynamics consist of pre-stall modes affected by the background flow field, driven by the blade-row performance.

Conclusion

Recalling Figure 3-2 and the expression of the growth rate obtained from Moore-Greitzer model, the effects of changes in loss on compressor performance and stability are as follows: a shift of the loss level will have an impact on performance (ψ will be changed) but stability, directly linked to the slopes ($\partial L/\partial \phi$), will not be affected. On the other hand, a modification of blade-row operating range (incidence range between two points where losses are twice the minimum losses - this expression is used to describe the width of the loss buckets) will change the slopes distribution ($\partial L/\partial \phi$) and eventually affect compressor stability.

3.2 Demonstration of Blade-Row Contribution to Compressor Dynamics

In this section, the dynamic compression system model is implemented as well as the mean line calculation presented in Chapter 2. Results presented were obtained for the 3-stage, repeating-stage compressor where the geometry is given in Appendix B. Changes in the loss distribution of the first-stage-rotor are studied in order to assess the contribution of blade-row performance on the compressor dynamics.

Introduction of a Loss Level Change: Performance is Altered, not Stability

This section presents the results of a loss bucket modification for rotor 1 of the 3-stage compressor in terms of loss level. A bias $\Delta\omega$ was artificially introduced on the loss bucket of rotor 1: $\omega = f(i)$, other blade-row loss buckets were kept unchanged. Figure 3-3 shows the baseline and

modified losses $\mathbf{L} = f(\phi)$ for all the blade-rows with the resulting bias $\Delta L = 0.01$. Note that the conversion from ω in the compressible mean line calculation to L in the incompressible dynamics calculation make the bias ΔL not perfectly constant over the entire flow coefficient range. However, the loss level change turns out to be modified by at most 1% for that flow range, which can be considered as a constant bias. On that figure, as well as on all the following, the circle (o) indicates the flow coefficient at which the compressor goes unstable (the real part or growth rate of the least stable eigenvalue becomes positive), and the asterisk (*) the design point.

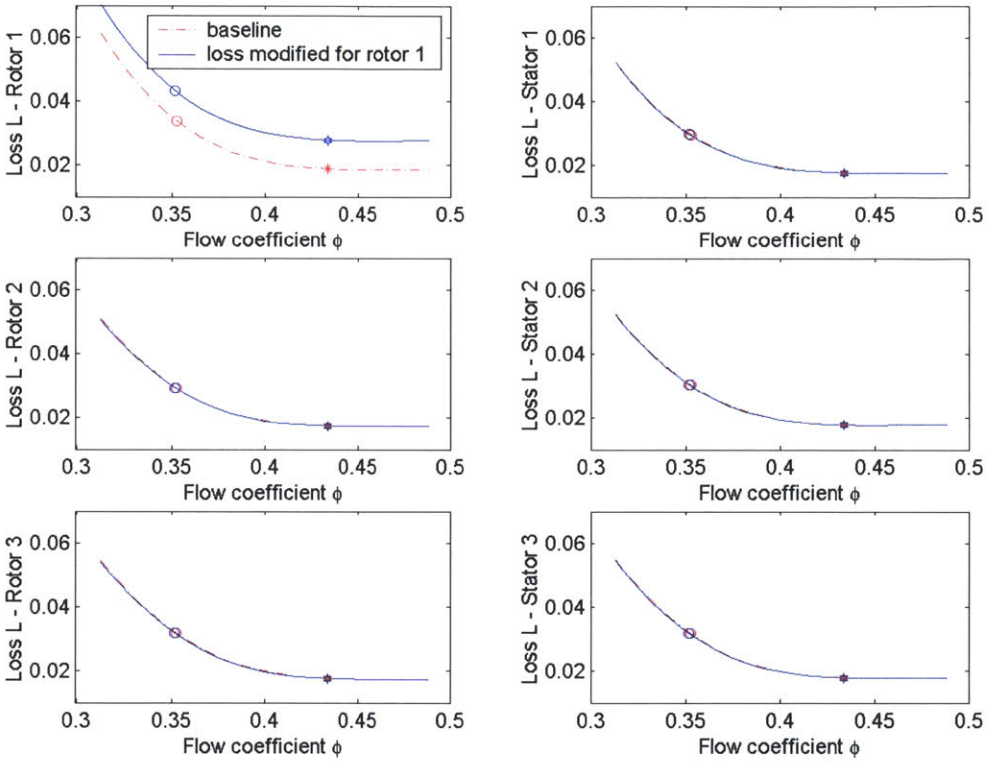

Figure 3-3: Blade-row loss buckets of the 3-stage, repeating-stage compressor – baseline and with modifications to rotor 1.

Figure 3-4 shows that the characteristics are shifted compared to each other and the impact of the loss level change for rotor 1 on the point where the compressor goes unstable is negligible (the difference between ϕ_{stall} with the baseline loss and the modified loss is 0.2% due to compressibility effects stemming from the mean line calculation).

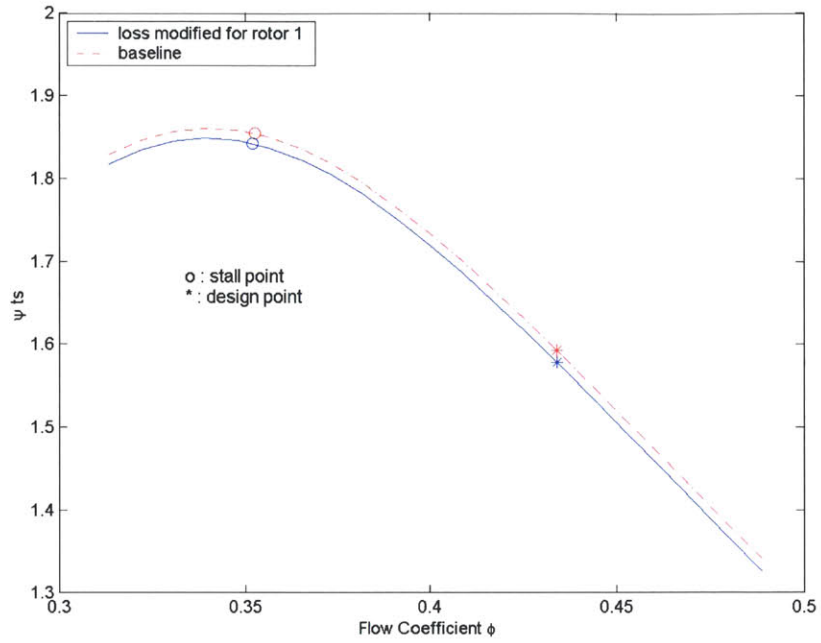

Figure 3-4: Characteristics of the baseline 3-stage compressor and of the compressor with modifications to rotor 1.

The outputs of this calculation are summarized in Table 3-1

	ψ_{design}	Efficiency	Stall Margin	$\Delta\phi$
Baseline	1.593	0.94	21%	0.063
Rotor 1 losses modified	1.578	0.93	21%	0.063

Table 3-1: Comparison of performance and stability between baseline and modified configuration.

As expected, a bias introduced on the loss bucket of one of the blade-rows leads to a modification of performance (pressure rise and efficiency) whilst stability is not altered.

Modification of the Slopes of the Loss Buckets: Stability is Altered, not Pressure Rise at Design Point

Figure 3-5 presents the loss bucket slope modification for rotor 1 of the 3-stage, repeating-stage compressor: $\partial L/\partial\phi$, i.e. the sensitivity to changes in flow coefficient, is modified for the loss of rotor 1. To obtain the change in $\partial L/\partial\phi$, a change in the loss slopes $d\omega/di$ (change in the width of the

blade-row loss bucket) was artificially introduced on the loss bucket of rotor 1 while keeping other loss buckets unchanged. Due to compressibility effects in the mean line calculation, the slopes $\partial L/\partial\phi$ of other blade-rows are also affected by the loss bucket modification of rotor 1, although the impact is limited (less than 1% of the loss levels)

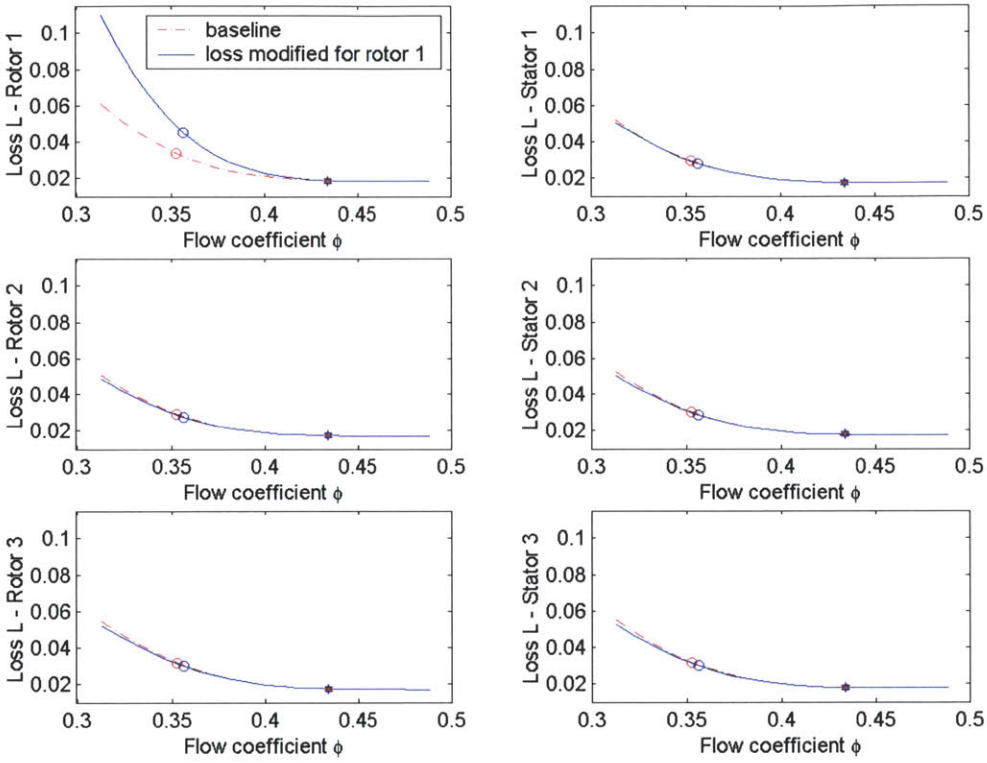

Figure 3-5: Blade-row loss buckets of the 3-stage, repeating-stage compressor – baseline and with modifications to rotor 1.

Figure 3-6 presents the characteristics of the 3-stage baseline compressor and the compressor with modified losses. The change in loss slopes directly affects stability while the compressor undergoes no pressure rise change at the design point.

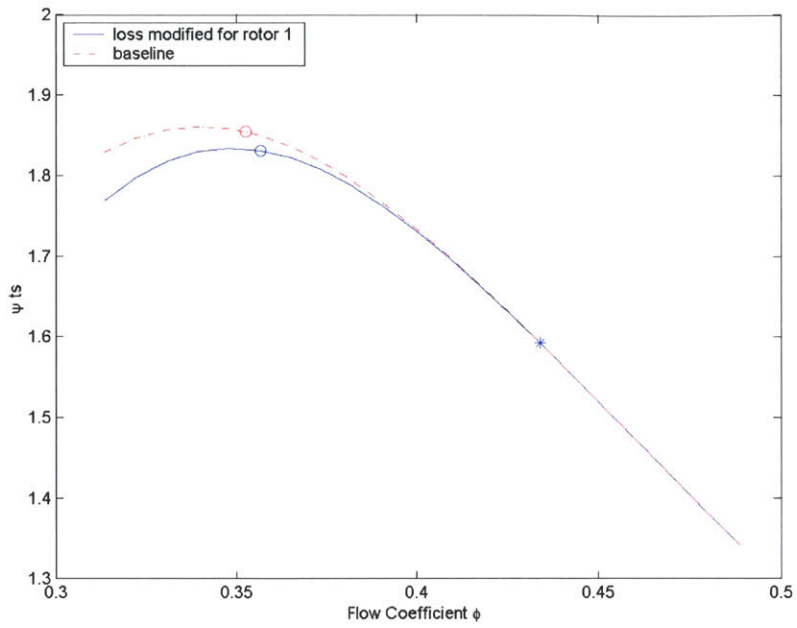

Figure 3-6: Characteristics of the baseline 3-stage compressor and of the compressor with modifications to rotor 1.

The outputs of this calculation are finally summarized in Table 3-2.

	ψ_{design}	Efficiency	Stall Margin	$\Delta\phi$	ψ_{peak}
Baseline	1.593	0.94	21%	0.063	1.854
Rotor 1 losses modified	1.593	0.94	20%	0.059	1.831

Table 3-2: Comparison of performance and stability between baseline and modified configurations.

Modifying the width of the loss buckets has no impact on pressure rise and efficiency at the design point (since the characteristics go through the same design point), but has an impact on stability because the slopes $\partial L/\partial\phi$ directly affect the dynamics: the steeper the loss slopes, the less stable the system. Furthermore, the change in $\partial L/\partial\phi$ entails a change in the operating range $\Delta\phi$ and in the peak pressure rise.

Conclusions

This preliminary analysis, as well as benchmarking the implementation of the dynamic compressor model, showed that in order to modify performance and stability for a given compressor in the light of the optimization procedure, one needs to find a way of modifying the blade-row losses

in two different ways. First, a way of introducing a change in the level of the losses (a reduction of the losses level leads to a rise in performance) has to be found. Second, one must be able to alter the sensitivity of blade-row stagnation pressure loss to flow angle or flow coefficient changes: an increase in width entails a rise in stability margin.

These conclusions lead into the next chapter where a scheme is established to alter blade-row performance through the modification of geometric parameters of the compressor blades.

Chapter 4

Analytical Dependence of Blade-Row Losses on Blade Geometry

Although modifications of the loss level and slope distribution were implemented in the previous chapter without any link to blades shape, the losses and the blade-row geometry are closely linked: any loss bucket modification is directly influenced by modifications in blade-row shape.

In the optimization framework presented in Figure 1-6, a relation between changes in loss bucket (or blade performance) imposed by the optimizer and changes in blades geometry is needed for the loop to be closed (symbolized by the function f). The need to define such a function f leads to an inverse design problem, i.e. a geometry that yields a prescribed loss distribution has to be found. This inverse design problem is non-trivial as there is not a unique relation between loss buckets and blade geometry. There is more than one gas-path / blade geometry combination that yields a single loss bucket since loss depends not only on the blade design philosophy, but also on installation (3-D effects, end-wall boundary layers, blade-row interactions, etc.).

Within the framework of this thesis, an attempt is made to find a relation leading from changes in blade geometry to loss bucket modifications for a given family of designs. Geometric parameters that influence loss distribution are suggested. Using the blade-to-blade flow solver MISES, losses are determined for a baseline geometry. Then, the baseline geometry is perturbed leading to the determination and assessment of sensitivities using MISES again. Sensitivities are important to be computed as they enable one to assess the effects of the perturbations on stability.

This chapter gives, first, a review of the geometric parameters that can be thought of in order to modify the shape of the loss buckets. Then the so-called blade channel modification, chosen to be a well-suited change in geometry linked to loss modifications inside the optimization loop, is introduced. Section 4.2 finally shows how the link between geometry and losses is quantified (in

order to be implemented in the optimization loop) based on interpolated calculations performed with the flow solver MISES.

4.1 Possible Geometric Modifications Influencing the Shape of a Blade-Row Loss Bucket

Several geometric modifications of the blades are presented in this section. Some modifications in geometry were used in recent optimization papers ([2] and [12]) and are of interest for future work. In these papers, camber line and thickness distribution modifications as well as blade chord changes were implemented. A high number of design variables was required to properly parameterize the blade shapes. Büche et al. ([2]), represented the blade geometry using Bezier curves describing the leading edge, trailing edge, suction side and pressure side of a blade. This approach led to a total of 19 parameters to define a blade section. Sieverding et al. [12] defined the blade geometry using the superposition of camber line and thickness distributions, described by Bezier and linear curves. This approach led to 20 parameters to define a blade section.

4.1.1 Camber Line Modification: Main Influence on the Slope Distribution of the Loss Buckets

The camber line of an airfoil has an impact on the width of the loss buckets. Cumpsty [3] shows data of airfoils with circular arc camber line, parabolic arc camber line and of a double circular arc airfoil. The main effect of these types of camber line modifications is sketched in Figure 4-1. The change in operating range between different configurations is due to a change in pressure distribution on the suction surface of the blades. The steeper the adverse pressure gradient on the suction side, the earlier separation occurs.

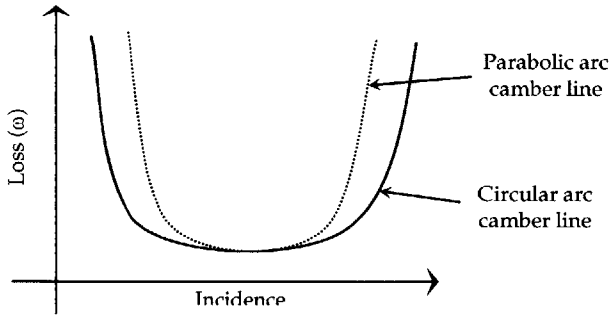

Figure 4-1: Influence of airfoil camber line on stagnation pressure loss (adapted from [3]).

4.1.2 Thickness Modification

The airfoil thickness also influences the shape of the loss buckets in terms of operating range. The main idea of a thickness modification is to re-shape the pressure distributions on the blade surface in order to delay boundary layer separation. Diffusion can be controlled by modifying the thickness distribution along the chord. Controlled diffusion aims at delaying the rise in loss due to a Mach number increase. This effect is sketched in Figure 4-2.

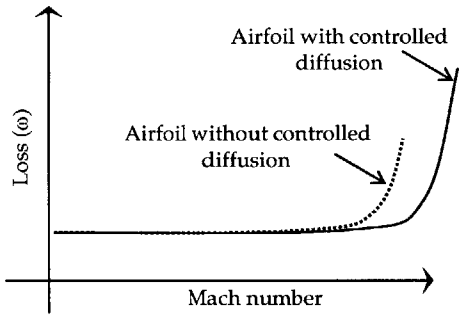

Figure 4-2: Influence of airfoil thickness on stagnation pressure loss (adapted from [3]).

4.1.3 Blade Chord Effects on the Minimum Loss Level

The chord of an airfoil impacts the loss bucket shape as follows: an increase in chord results in an increase in the airfoil surface, hence in the profile drag (leading to higher losses). This can be represented by a bias effect (a change in the overall loss level) as sketched in Figure 4-3.

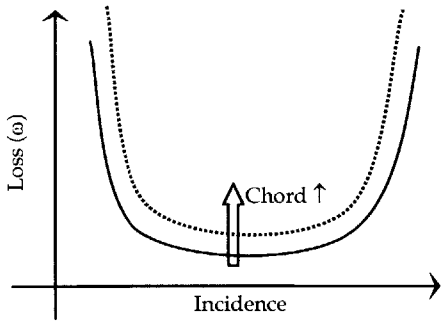

Figure 4-3: Influence of airfoil chord on stagnation pressure loss.

However, this effect is quite limited in the range of chord and velocity values used for the compressors to be optimized (operating at low speed). A typical value for the relative velocity at the inlet of a blade-row is about 150 m/s, a typical chord value is 2 cm, leading to a Reynolds number of about Re = 2.10^5. Cumpsty presents in [3] experimental data about the effect of Reynolds number on blade performance. It is shown that for such Reynolds numbers, even an increase in chord by 200% leads to loss variation of less than 15%. In other words, Reynolds number effects or chord effects have limited impact on blade-row loss and seem not to lead to any effective design variables.

4.1.4 Modifications to the Blade Channel

The last geometric change is the so-called blade channel modification. It consists of re-staggering the blades: the blades are hinged at the leading edge entailing alterations of the flow incidence and of the properties of the blade channel (area ratio, diffusion factor). The blade channel modification will be described and analyzed with more detail in the next sections.

This particular modification is to be linked to changes in loss inside the optimization loop. The change in the blade channel angle is of interest for two reasons. First, it leads to a combination of changes in the level and the width of the loss buckets. Both of these changes are needed (see Chapter 3) to introduce alterations in performance and stability. The afore-presented shape modifications on the contrary led to a single type of change (either level or slopes distribution). Second, it fulfills the limitation imposed by the version of the optimizer **Isight** available (academic Beta version). The optimization software is limited to 8 design variables. It does not provide all the freedom necessary to implement geometric changes parameterized by a high number of variables (like camber changes or thickness changes as presented in [2] and [12]). The blade channel modification is chosen to cope with that issue, as it is an effective way of changing geometry, and is simple to be parameterized. Only one design variable per blade-row is necessary (hence for the 3-stage, repeating-stage compressor to be optimized, a total of 6 design variables will be implemented).

4.2 Practical Implementation of Modifications to the Blade Channel

4.2.1 Geometric Implementation

Modifications to the blade channel (denoted Δ_{bc}) imply the following: the blade is hinged at the leading edge and for a given change of Δ_{bc} in degrees, the following blade properties are modified:

- inlet metal angle ($\beta^{inlet}_{metal\,new} = \beta^{inlet}_{metal} + \Delta_{bc}$)
- outlet metal angle ($\beta^{outlet}_{metal\,new} = \beta^{outlet}_{metal} + \Delta_{bc}$)

- stagger angle ($\gamma_{new} = \frac{\beta^{inlet}_{metal\ new} + \beta^{outlet}_{metal\ new}}{2} = \gamma + \Delta_{bc}$)

Figure 4-4 illustrates a modification of the blade channel. This purely geometric modification of the blade channel leads to flow changes in terms of diffusion factor, turning and area ratio. These flow changes are determined and described below.

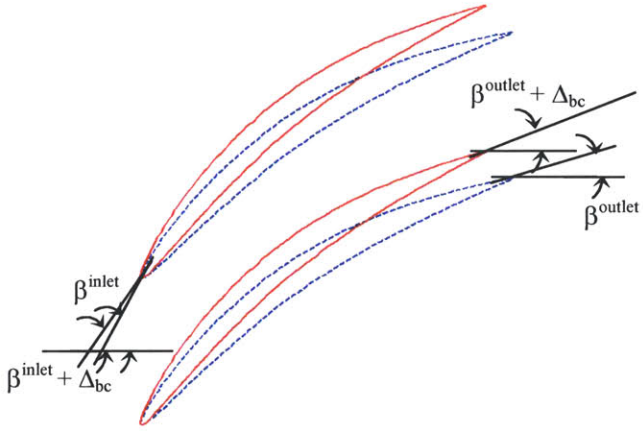

Figure 4-4: Illustration of modifications to the blade channel.

4.2.2 Effect of Modifications to the Blade Channel on Blade-Row Loss: Diffusion Effects

An example of how the blade channel modification affects the loss bucket is presented and discussed. The results are based on numerical calculations with the quasi-3D blade-to-blade flow solver MISES. This solver was developed by Youngren and Drela [18] and used by Lavainne [9] whose framework was implemented to perform calculations in this thesis. The blade geometry files were generated using XFOIL (Drela [5]). The loss coefficients computed with MISES are defined from the hypothetical mixed-out state downstream the blade-row considered for the calculation (see [18]).

The blades studied are presented in Table 4-1 listing their metal and stagger angles. A NACA 0012 profile is used for all these blades with a camber of 9% of the chord. The original blade is referred to as baseline and the other ones have a modified blade channel: Δ_{bc}= +3° and Δ_{bc}= -3°.

	Baseline	Δ_{bc}= +3°	Δ_{bc}= -3°
Inlet metal angle	59°	62°	56°
Outlet metal angle	25°	28°	22°
Stagger angle	42°	45°	39°

Table 4-1: Blade geometry.

For these blades, the following loss buckets (Figure 4-5) were computed using MISES at low Mach numbers (around $M = 0.1$). The results are presented next. The diffusion factor (DF) is defined as

$$DF = 1 - \frac{V_2}{V_1} + \frac{|v_2 - v_1|}{2\sigma V_1}, \tag{4.1}$$

where all the velocities V and v (tangential velocity) are defined in the frame of reference of the considered blade, and where σ is the blade-row solidity (for more details, refer to Kerrebrock [8]).

Furthermore, the turning (difference between the relative flow angles at trailing edge and leading edge) and the area ratio (areas are normal to the flow in blade passages at leading and trailing edge) are given in Table 4-2 for each blade at an incidence of 1.6° (close to the incidence of minimum loss for the three configurations).

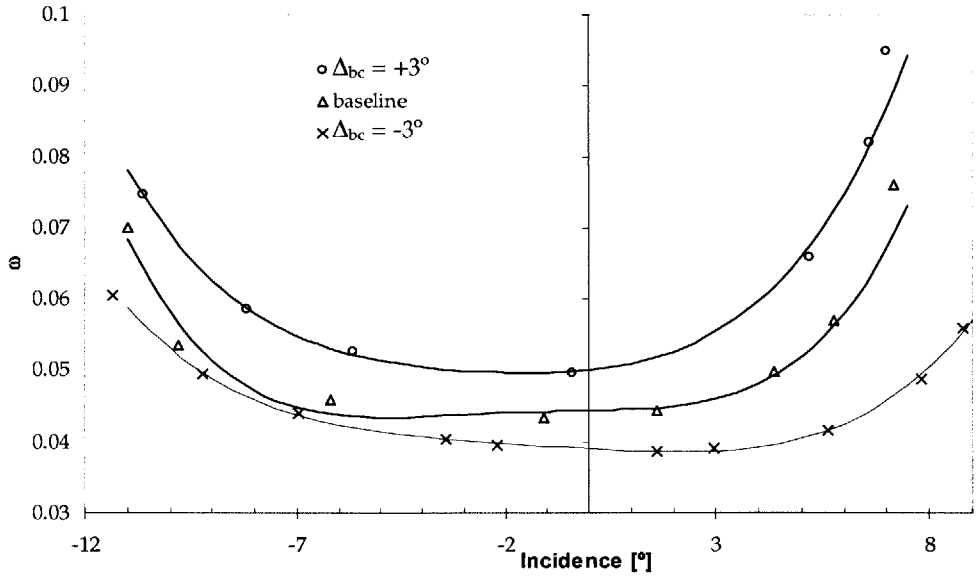

Figure 4-5: Loss buckets for the blades studied.

	Δ_{bc}= -3°	Baseline	Δ_{bc}= +3°
DF	0.482	0.537	0.546
Turning	28.3°	28.3°	26.6°
Area ratio (inlet/outlet)	0.603	0.568	0.532

Table 4-2: Blade DF, turning and area ratio at 1.6° incidence.

It is clear from Figure 4-5 that the so-called blade channel modification triggers two effects on the loss buckets: introduction of a loss level modification at a given incidence as well as introduction of an operating range change. Table 4-2 elucidates these results. An increase in the blade channel angle leads to an increase in the diffusion factor because of the area ratio reduction with Δ_{bc}. The area ratio (inlet / outlet) is reduced when the blade channel angle is increased, hence the ratio V_2/V_1 is decreased when a positive Δ_{bc} is imposed. This velocity ratio directly influences the second term present in the expression of the diffusion factor (equation (4.1)). This diffusion effect entails an increase in the boundary layer thickness when the blade channel angle is increased (diffusion factor and boundary layer thickness are closely linked as described in [8]). That thickening of the boundary layer finally explains the higher loss as well as the lower turning for higher blade channel angles. The decrease in the area ratio also explains the fact that the incidence range decreases when the blade channel modification is positive. The adverse pressure gradient the flow is subject to increases with Δ_{bc} and hence flow separation occurs at lower incidence when Δ_{bc} is increased.

Note that all the flow modifications due to changes in blade channel angles are described on blades that see the flow with the same incidence. This detail has to be kept in mind since blade-row incidences are also altered for a given flow coefficient on a compressor (the inlet metal angles depend on the blade channel angles). The incidence change adds a shift in the loss function of the flow coefficient. This phenomenon will be described in more depth in Chapter 5.

4.2.3 Least Squares Interpolation Between Losses, Incidence and Δ_{bc}

From these computations, a numerical relation between blade channel modification, loss and incidence has to be found in order to define the function f depicted in Figure 1-6 and introduced in this chapter. For that purpose, an analysis of the data has to be carried out prior to the optimization process. This is sketched in Figure 4-6.

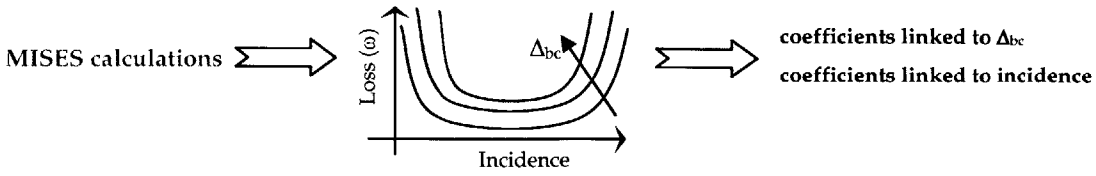

Figure 4-6: Preliminary analysis to determine an analytical relation between 2D blade-row loss and blade channel geometry.

This preliminary analysis consists of a least squares interpolation and aims at obtaining an optimal fit of the data with small relative errors. The following polynomial relation can be used

$$\omega(\mathbf{i},\Delta_{bc}) = c_0 + c_1 \cdot \mathbf{i} + c_2 \cdot \Delta_{bc} + c_3 \cdot \Delta_{bc} \cdot \mathbf{i} + c_4 \cdot \mathbf{i}^2 + c_5 \cdot \mathbf{i}^3 \cdot \Delta_{bc} + c_6 \cdot \mathbf{i}^4,$$

and can be re-arranged to yield:

$$\omega(\mathbf{i},\Delta_{bc}) = (c_0 + c_2 \cdot \Delta_{bc}) + (c_1 + c_3 \cdot \Delta_{bc}) \cdot \mathbf{i} + c_4 \cdot \mathbf{i}^2 + (c_5 \cdot \Delta_{bc}) \cdot \mathbf{i}^3 + c_6 \cdot \mathbf{i}^4.$$

Such a relation will potentially capture the shape of the computed data surface well. A low order linear relation in Δ_{bc} only is introduced (c_2) to represent the effect of blade channel variation on the overall loss level. A coupling term between **i** and Δ_{bc} is also considered (c_3) to take into account potential twist of the resulting surface. Δ_{bc} is also coupled with a higher order term in **i** so as to model the operating range modification that goes along with blade channel variation. Finally, it can be noted that low order terms only (1st order) are considered for the relation between ω and Δ_{bc} to avoid oscillations that could occur using higher order terms. On the other hand, high order terms are considered to model the relation between **i** and ω: the slopes of losses relatively to incidence are closely linked to stability as discussed in Chapter 3. Since stability is one of the optimization objectives, a high order relation is implemented between ω and **i** to keep the slopes of the interpolated data as close as possible to the computed data.

4.2.4 Example of Implementation of the Least Squares Interpolation

The interpolation method presented for a general case in the previous paragraph is now applied to the data discussed in section 4.2.2. The interpolation results are presented in Figure 4-7 and the norm of the residuals are presented for each of the loss buckets generated at different blade channel

angles in Table 4-3. The definition of the norm L_2 used here is given below. The square of this norm is minimized by the least squares method.

$$\|\cdot\|_2 : \Re^n \to \Re$$

$$x \mapsto \|x\|_2 = \sqrt{\sum_{i=1}^{n} |x_i|^2}$$

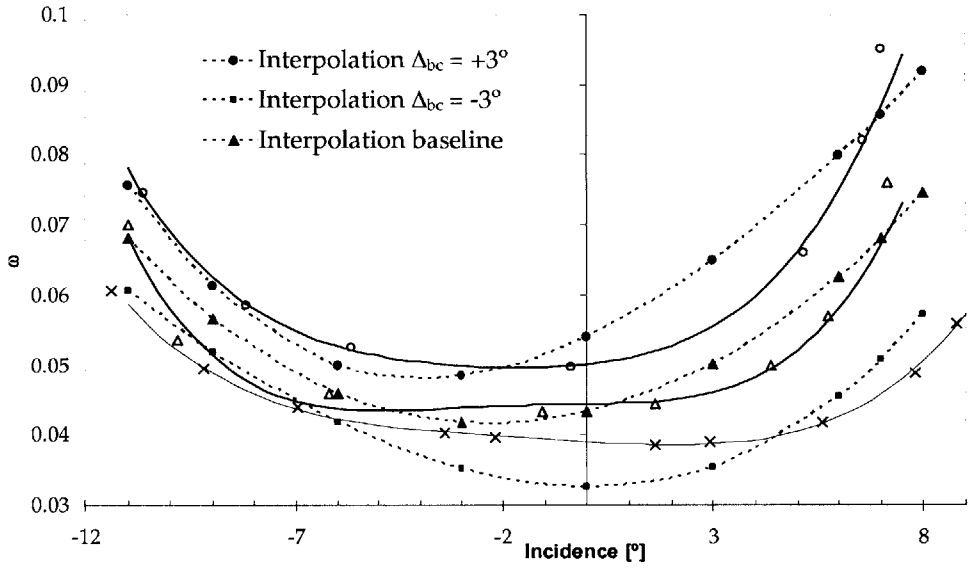

Figure 4-7: Loss buckets and their interpolation based on a least squares method.

	Δ_{bc}= -3°	Baseline	Δ_{bc}= +3°
L_2 norm of residual between computed and interpolated data	0.0257	0.0214	0.0318
L_2 norm of residual between the slopes of the computed and interpolated data	0.0088	0.0142	0.0186

Table 4-3: Comparison between computed and interpolated data for the three loss buckets shown in Figure 4-7.

Although the interpolated data can be used in the optimization process, there is a discrepancy: the slopes of the interpolated data do not follow precisely the actual slopes of the loss buckets.

In order to get a better fit of the slopes, another interpolation method should be used. The methodology can be summarized as follows:

- The numerical data for the baseline blade is fitted using a least squares method. It results in a polynomial interpolation up to the 4th order for the loss bucket function of incidence. The best fit is obtained using the relation:

$$\omega(\mathbf{i}) = \lambda_0 + \lambda_1 \cdot \mathbf{i} + \lambda_2 \cdot \mathbf{i}^2 + \lambda_3 \cdot \mathbf{i}^3 + \lambda_4 \cdot \mathbf{i}^4,$$

where the λ_i are determined using a least squares method.

- A linear relation is then established between the λ_i and the blade channel modification angle. Mathematically, a possible relation between loss, incidence and Δ_{bc} is:

$$\omega(\Delta_{bc}, \mathbf{i}) = \xi_o(\Delta_{bc}) \cdot \lambda_0 + \lambda_1 \cdot \mathbf{i} + \lambda_2 \cdot \mathbf{i}^2 + \lambda_3 \cdot \mathbf{i}^3 + \xi_1(\Delta_{bc}) \cdot \lambda_4 \cdot \mathbf{i}^4.$$

$\xi_i(\Delta_{bc})\ j \in \{0,1\}$ are coefficients only function of the blade channel modification angle Δ_{bc}. By definition, they are both set to 1 for the baseline case. It has to be noted that ξ_0 represents the loss level modification (or bias effect) since it is a coefficient of 0th order in the loss-incidence polynomial. ξ_1, on the other hand, captures the change in width of the loss buckets due to the blade channel modification angle, appearing as a coefficient multiplying incidence to the 4th power.

The results of this interpolation are presented in Figure 4-8 and Table 4-4.

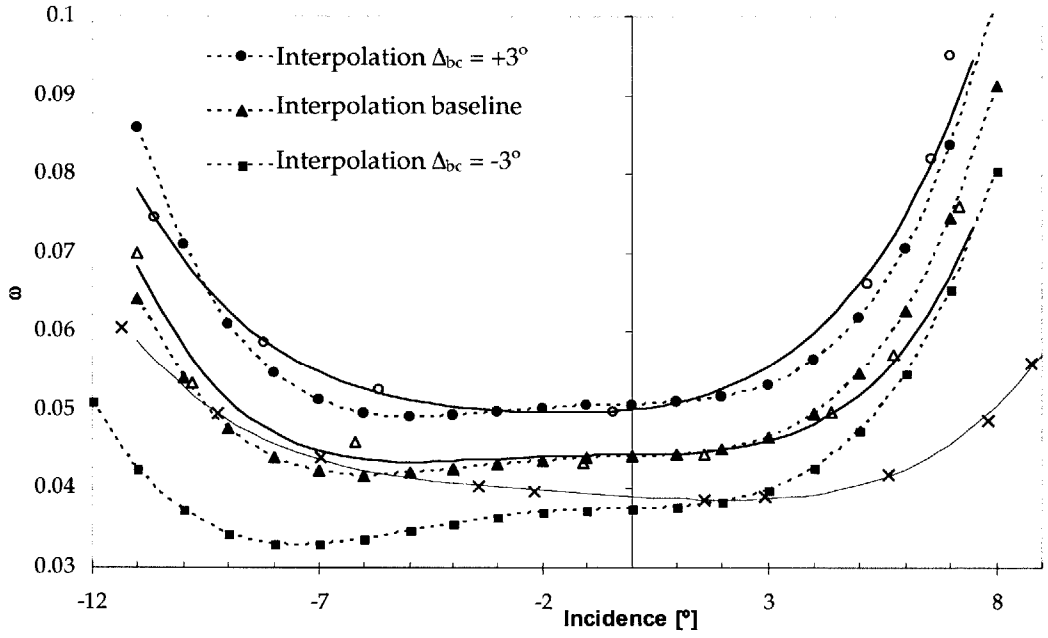

Figure 4-8: Interpolation of the computed loss data.

	Δ_{bc}= -3°	Baseline	Δ_{bc}= +3°
L_2 norm of residual between computed and interpolated data	0.0682	0.0218	0.0173
L_2 norm of residual between the slopes of computed and interpolated data	0.0217	0.0078	0.0116

Table 4-4: Comparison between computed and interpolated data for the three loss buckets.

For the baseline and Δ_{bc}= +3° configurations, the interpolation is much better (in terms of norm of the residuals) than the one using the least squares method. The slopes are closer to their actual computed values (the norm of the slope residuals is 45% lower for the baseline configuration using the new interpolation rather than the least squares interpolation, and 38% for the Δ_{bc}= +3° configuration), which means that the dynamic behavior is captured more accurately. On the other hand, obviously, the interpolation for the Δ_{bc}= -3° configuration is worse than the one obtained with the least squares method (residuals of the data and of the slopes are two-and-a-half times higher with the new interpolation method).

The second interpolation (as shown in Figure 4-8) is nonetheless the one implemented to obtain the results presented later in this chapter and used for the final proof-of-concept optimization (presented in Chapter 6). This interpolation captures the loss trend with blade channel modification in terms of operating range and loss level. In spite of the low quality of the interpolation for negative Δ_{bc}, the repercussions of that bad interpolation in the optimization results will be limited: the optimizer is expected to move the design variables to positive (and not negative) blade channel modifications leading to an improvement of stability (as explained in next chapter).

4.2.5 Another Possible Method to Interpolate the Computed Losses

Room is left to improve the correlation between loss, incidence and the angle of blade channel modification. Another way of analytically describing this correlation is proposed next, although not implemented because of time constraints.

Starting from the assumption that the baseline loss bucket can be interpolated using a 4th order polynomial, one can write:

$$\omega(\mathrm{i}) = \mathrm{A}\mathrm{i}^4 + B\mathrm{i}^3 + \mathrm{C}\mathrm{i}^2 + D\mathrm{i} + E.$$

The five coefficients A, B, C, D and E have to be determined. For that purpose, the loss bucket is imposed to go through three particular points as depicted in Figure 4-9: the point where the loss reaches its minimum value (ω_0, i_0) and the points where the loss reaches twice its minimum level (ω_1, i_1) and (ω_2, i_2). Furthermore, the point of minimum loss has to be the location where the slope $\partial\omega/\partial i$ is zero. The aforementioned constraints define four equations to determine five coefficients (A,

B, C, D, E). A constant is left to be adjusted via an iterative process in order to obtain the best fit of the baseline data.

After having defined the baseline characteristic, the effects of the modification of the blade channel angle have to be taken into account. For that purpose, a modulation of the loss levels at the minimum value (ω_0) and at twice the minimum value (ω_1 and ω_2) is implemented. The data is used to compute the sensitivities of the loss levels to the modification of the blade channel angle ($\partial\omega/\partial\Delta_{bc}$). Finally, shifts of the incidence at the minimum loss level (or at twice that level) also have to be included via the coefficients k, m, n (also determined from the data) as shown in Figure 4-9.

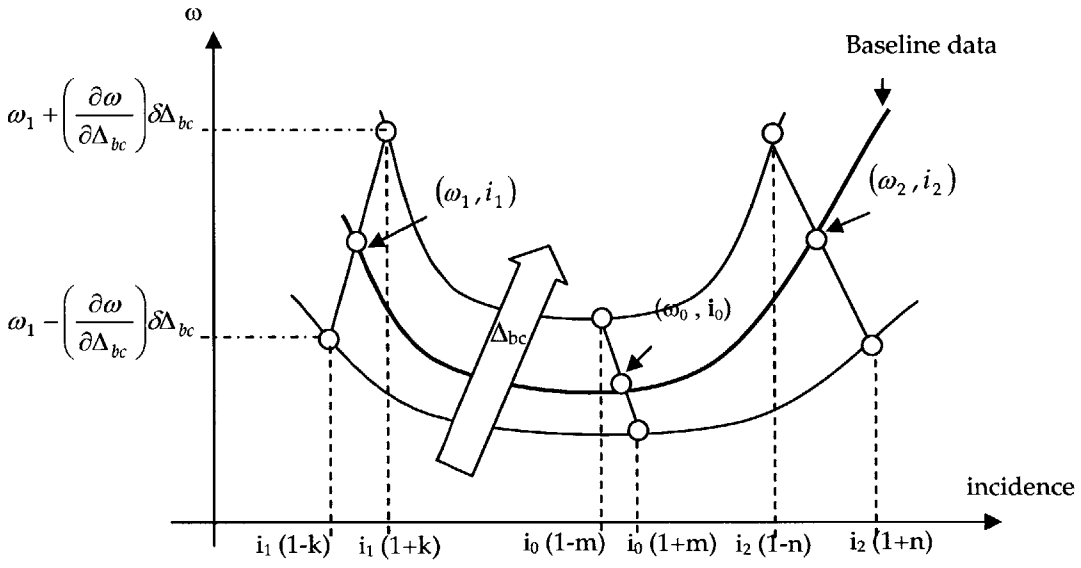

Figure 4-9: Schematic of a method to analytically describe the computed blade-row losses.

4.3 Conclusion

This chapter introduced several geometric modifications to blade-row geometry and their effects on stagnation pressure loss. Modifications of the blade channel angle are to be implemented inside the optimization framework. The effects of modifications of blade channel angles on losses were computed and explained. Several methods were presented to analytically describe the computed data and one was chosen for the optimization. The analytical description of the data provides a solution to the inverse design problem introduced at the beginning of the chapter.

The final sketch shown in Figure 4-1 summarizes the steps conducted using the optimizer. Starting with an original loss bucket, the optimizer specifies a new set of coefficients (ξ_0,ξ_1) that

modifies the bucket shape. These coefficients also determine the blade-row geometry. In the light of the analytical description of the data, a loss bucket change quantified by the coefficients ξ_0 and ξ_1 are strictly equivalent to a quantified modification of the blade channel angle, in such a way that (ξ_0,ξ_1) and Δ_{bc} can be considered as the design variables in the optimization loop. In other words, there is only one degree of freedom: a single set of coefficients (ξ_0,ξ_1) describes one value of Δ_{bc}.

It is still necessary to carry out a sensitivity analysis to find out what magnitude should be given to Δ_{bc} and to analyze in more depth what effects it has on the overall performance and stability of a given compressor.

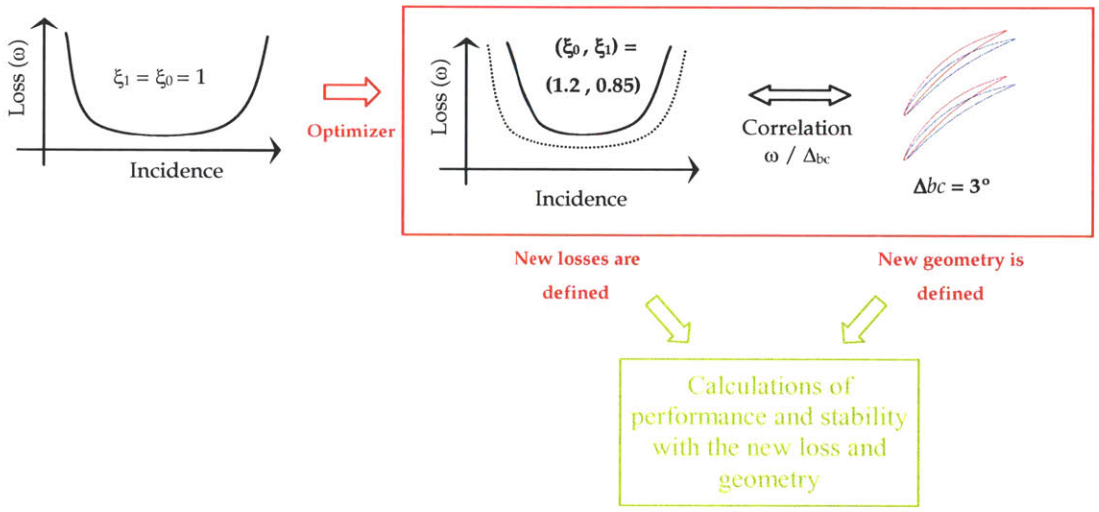

Figure 4-10: Example of implementation of the blade channel / loss relation.

Chapter 5

Assessment of Effects of Blade Channel Modifications on Compressor Performance and Stability

The inversely-optimized compressor design for enhanced stability involves the determination and alteration of compressor system dynamics. The compressor dynamics consist of pre-stall modes which are affected by the background flow-field, meaning that there is a direct link between dynamic modes, blade-row performance and blade-row geometry. To facilitate the optimization, one needs to assess its feasibility, i.e. determine the sensitivity of compressor dynamic behavior to changes in blade-row performance and the sensitivity of blade-row performance to changes in geometry. These sensitivities will eventually guide the optimization strategy and procedure to be implemented.

This chapter discusses and analyzes the above mentioned sensitivities: the effects on compressor performance and stability of loss changes induced by modifications of the blade channel angle are determined (first profile loss only, then profile and end-wall loss). The results presented in this chapter are used in the optimization framework.

5.1 Analysis of the Sensitivity of Compressor Performance and Stability to Blade Channel Modifications - Profile Loss Only

The analysis presented in this section is carried out with the mean line calculation coupled to the dynamic compression system model which was introduced in Chapter 2: the optimization loop without end-wall effects. Hence, profile loss is the only loss mechanism taken into account for now.

5.1.1 Qualitative Analysis

First, a qualitative description is given elucidating the effects on the compressor if only the blade channel of rotor 1 is modified by +3°.

The blade channel modification results in the following changes, in terms of blade-row loss:

- The rotor 1 loss bucket as a function of flow coefficient is modified, due to two effects. First, the loss slopes and loss levels are changed, directly due to the blade channel modification. Secondly, this effect being the most important, a shift of the loss bucket occurs due to an incidence change as a consequence of the geometric modification (the blade's leading edge metal angle and the incidence are modified). In the present case, the positive blade channel modification leads to a decrease in incidence for rotor 1. The aforementioned phenomena add up and lead to an altered loss bucket for the modified blade-row as shown in Figure 5-1.

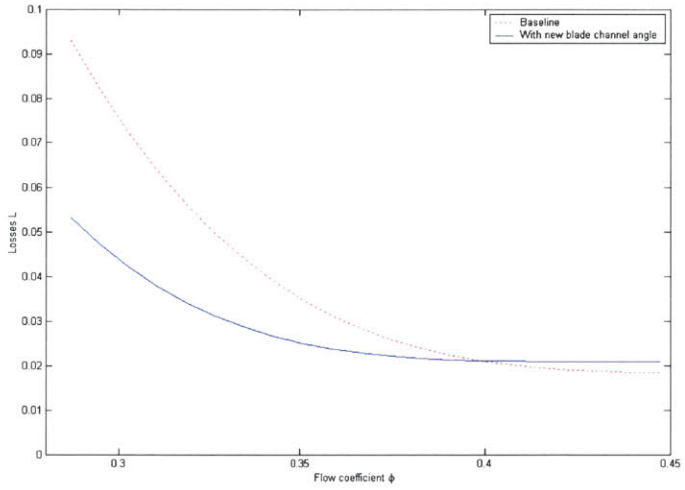

Figure 5-1: Rotor 1, baseline and with a blade channel angle change of Δ_{bc} = +3°, loss bucket as a function of flow coefficient.

- Figure 5-2 shows that the losses of the blade-row adjacent to the blade-row which has a modified geometry (in that case, stator 1) are also affected. This is because the blade channel modification also entails a metal angle change at the exit of rotor 1, leading to different flow conditions at the inlet of stator 1. This also entails a change in the diffusion factor which is quantified in next section. The stagnation pressure loss of the blade-rows downstream stator 1 is not affected.

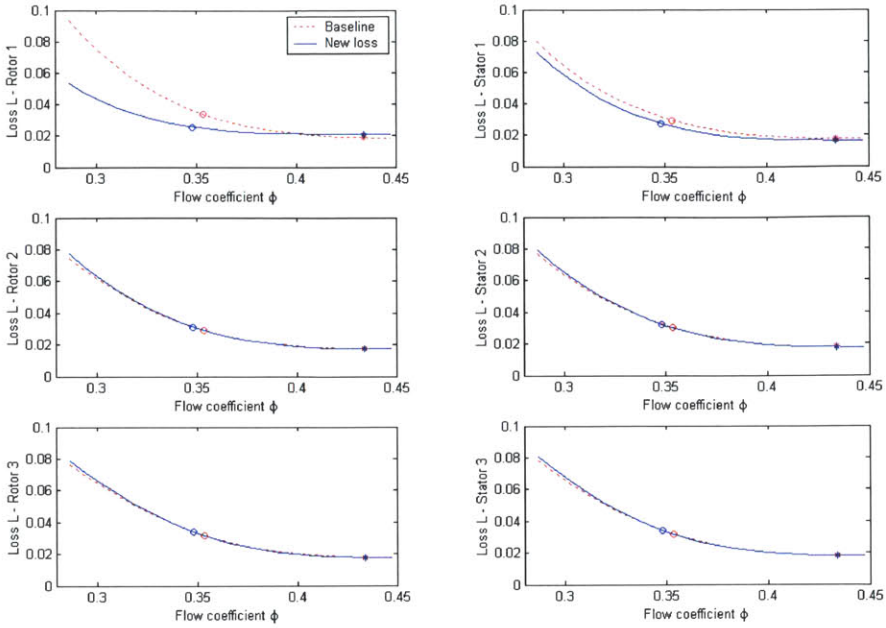

Figure 5-2: Loss buckets as the function of flow coefficient for the baseline compressor and modified compressor.

Finally, Figure 5-3 shows the characteristics of the baseline and modified compressors. The blade channel modification results in a change of the slope ($\partial\psi/\partial\phi$) that alters the pre-stall dynamics: stall occurs in this example at a higher flow coefficient due to the positive Δ_{bc} = +3°. The performance is also affected by the modification of the loss level.

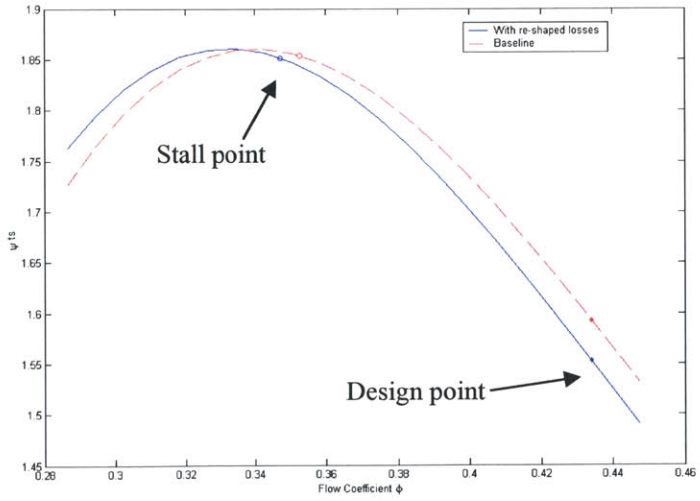

Figure 5-3: 3-repeating-stage compressor characteristics - baseline compressor and with a blade channel angle change of Δ_{bc} = +3° for rotor 1.

5.1.2 Quantitative Analysis

In this section, the performance and dynamic stability of the baseline 3-stage, repeating-stage compressor are given and compared to several modified configurations. At the design point, the overall pressure ratio is **OPR = 1.349**, the adiabatic efficiency is **η = 0.936** and the stall margin **SM = 20.9%**. The pressure ratio has a typical value for a 3-stage compressor; the design point is chosen such that the stall margin is around 20%. As for the adiabatic efficiency, the value obtained is high because only profile loss is taken into account and end-wall or secondary losses are not included. Including such additional losses would lead to more typical values of the efficiency neighboring 0.85 (see Figure 3-1).

First, a blade channel modification of rotor 1 is analyzed.

R1	*S1*	*R2*	*S2*	*R3*	*S3*	*OPR*		*η*		*SM*	
$\Delta_{bc}=+3^o$	-	-	-	-	-	**1.342**	**-0.5%**	**0.934**	**-0.2%**	**22.5%**	**+1.6**
$\Delta_{bc}=-3^o$	-	-	-	-	-	**1.356**	**+0.5%**	**0.936**	**0%**	**19.0%**	**-1.9**

Table 5-1: Sensitivity analysis of rotor 1 modification.

Table 5-1 quantifies the effect of blade channel modifications on performance and stability. As expected from the loss curves presented in Figure 5-1, a positive blade channel modification leads to a rise in stall margin and a decrease in performance. The stability improvement stems from the fact that the rise in the slopes ($\partial\psi/\partial\phi$) happens at a lower flow coefficient due to the incidence reduction. This incidence change leads to a diffusion factor (defined in equation 4-1) change that follows the expected trend as shown in Table 5-2.

	Diffusion factors					
	R1	*S1*	*R2*	*S2*	*R3*	*S3*
Baseline configuration	0.596	0.576	0.575	0.582	0.581	0.537
Rotor 1 $\Delta_{bc}=+3^o$	**0.574**	0.555	0.572	0.579	0.577	0.534
Rotor 1 $\Delta_{bc}=-3^o$	**0.615**	0.594	0.578	0.584	0.584	0.54

Table 5-2: Effects of rotor 1 blade channel modifications on the diffusion factor of the blade-rows.

Table 5-2 shows that a 3° blade channel modification (either positive or negative) approximately leads to a 3.5% change in diffusion factor (DF is increased if Δ_{bc} is negative and vice versa) for the

blade-row which has a modified geometry. Stator 1 undergoes a diffusion factor change of the same magnitude due to the flow modification entailed by the change in the exit angle of rotor 1. The other blade-rows downstream have their diffusion factor almost not affected (less than 0.6%). Figure 5-2 can also be referred to since it illustrates the aforementioned quantitative results.

Table 5-3 and Table 5-4 present the same results for a blade channel modification of stator 1. These results lead to the same comments as those made for rotor 1.

R1	*S1*	*R2*	*S2*	*R3*	*S3*	*OPR*		*η*		*SM*	
-	$\Delta_{bc}=+3^o$	-	-	-	-	1.342	-0.5%	0.934	-0.2%	23.0%	+2.1
-	$\Delta_{bc}=-3^o$	-	-	-	-	1.356	+0.5%	0.936	0%	18.0%	-2.9

Table 5-3: Sensitivity analysis of stator 1 modification.

	Diffusion factors					
	R1	*S1*	*R2*	*S2*	*R3*	*S3*
Baseline configuration	0.596	0.576	0.575	0.582	0.581	0.537
Stator 1 $\Delta_{bc}=+3^o$	0.596	**0.553**	0.555	0.579	0.576	0.534
Stator 1 $\Delta_{bc}=-3^o$	0.596	**0.596**	0.594	0.584	0.584	0.54

Table 5-4: Effects of stator 1 blade channel modifications on blade-row diffusion factor.

Geometric changes applied to other blade-rows have the same effects as those presented above for rotor 1 and stator 1. This is expected since the compressor has repeating stages and incompressible flow conditions. However, the last stator has a lower effect on performance and stability since it does not affect any downstream blade-row.

Finally, the impact of a modification of the blade channel of all blade-rows is quantified. The results are summarized in Table 5-5.

R1	*S1*	*R2*	*S2*	*R3*	*S3*	*OPR*		*η*		*SM*	
$\Delta_{bc}=+3^o$	$\Delta_{bc}=+3^o$	$\Delta_{bc}=+3^o$	$\Delta_{bc}=+3^o$	$\Delta_{bc}=+3^o$	$\Delta_{bc}=+3^o$	1.312	-2.7%	0.925	-1.2%	33.2%	+13.3
$\Delta_{bc}=-3^o$	$\Delta_{bc}=-3^o$	$\Delta_{bc}=-3^o$	$\Delta_{bc}=-3^o$	$\Delta_{bc}=-3^o$	$\Delta_{bc}=-3^o$	1.38	+2.3%	0.933	-0.3%	8%	-12.9

Table 5-5: Sensitivity analysis of compressor-wide modifications.

5.1.3 Conclusions

The following conclusions can be drawn:

- All the blade-rows show the same behavior: an increase in the blade channel angle leads to a loss of performance and a gain of stability explained by a diffusion factor reduction. On the other hand, a decrease in the blade channel angle leads to a gain of performance and a loss of stability.
- An optimization is needed to find a trade-off between performance and stability: an increase in stability is reached to the detriment of performance and vice versa.
- Modifications of the blade channel angles ranging from -3° to +3° lead to the following magnitudes of variations: 5% of the overall pressure ratio baseline value, 1.5% of efficiency and 25.2% of stall margin. It seems that the evolution of Δ_{bc} between [-3° ; +3°] is reasonable as the impact on stability is noticeable (stall margin ranging from 8% to 33.2%). However, the performance change is limited, and larger changes in blade channel angles could also be tried whilst performing an optimization.

5.2 Analysis of the Sensitivity of Compressor Performance and Stability to Blade Channel Modifications - Profile and End-Wall Loss

A similar analysis compared to the one in previous section is conducted. It aims at assessing the impact of the addition of end-wall effects on compressor performance and stability. It also aims at devising an optimization strategy. Given all the limitations presented in Chapter 2, it might be relevant or not to include the end-wall correlations in the optimization loop. It might be enough to apply the corrections due to end-wall effects once the optimization process without end-wall correlations is performed (see Figure 5-4). The following paragraphs discuss this dilemma.

The 3-stage, repeating-stage compressor is used again for this analysis. First, the compressor performance and stability are computed including end-wall effects. The calculation procedure is described in Chapter 2 and the results are repeated here. At the design point, the overall pressure ratio is **OPR = 1.317**, the adiabatic efficiency is η **= 0.924** and the stall margin is **SM = 26.7%.**

Next, the results obtained after changes in the blade channel angle of rotor 1 only, stator 1 only, and all blade-rows simultaneously are presented.

R1	S1	R2	S2	R3	S3	OPR		η		SM	
$\Delta_{bc}=+3^o$	-	-	-	-	-	1.307	-0.8%	0.923	-0.1%	27.9%	+1.2
$\Delta_{bc}=-3^o$	-	-	-	-	-	1.327	+0.8%	0.923	-0.1%	25.4%	-1.3

Table 5-6: Impact of modifications of the blade channel angle of rotor 1 on performance and stability.

R1	S1	R2	S2	R3	S3	OPR		η		SM	
-	$\Delta_{bc}=+3^o$	-	-	-	-	1.308	-0.8%	0.923	-0.1%	28.5%	+1.8
-	$\Delta_{bc}=-3^o$	-	-	-	-	1.327	+0.8%	0.924	0%	24.4%	-2.3

Table 5-7: Impact of modifications of the blade channel angle of stator 1 on performance and stability.

R1	S1	R2	S2	R3	S3	OPR		η		SM	
$\Delta_{bc}=+3^o$	$\Delta_{bc}=+3^o$	$\Delta_{bc}=+3^o$	$\Delta_{bc}=+3^o$	$\Delta_{bc}=+3^o$	$\Delta_{bc}=+3^o$	1.272	-3.4%	0.917	-0.8%	35.3%	+8.6
$\Delta_{bc}=-3^o$	$\Delta_{bc}=-3^o$	$\Delta_{bc}=-3^o$	$\Delta_{bc}=-3^o$	$\Delta_{bc}=-3^o$	$\Delta_{bc}=-3^o$	1.368	+3.9%	0.918	-0.6%	15.4%	-11.3

Table 5-8: Impact of compressor-wide modifications of blade channel angles on performance and stability.

Adding end-wall loss effects to the stability and performance calculation leads to results similar to those obtained with only profile loss. Even though the magnitude of the variations in performance and stability are not exactly the same, similar trends are found: an increase in the blade channel angle leads to a decrease in performance and an increase in stability.

Furthermore, this analysis elucidates the strategy to be used in the optimization framework. It would be possible, as presented in Figure 5-4, to run either the optimization with the full calculation loop (mean line calculation, end-wall effects and compressor dynamics calculation at each optimization iteration, as presented in Chapter 2) or to run the optimization using a simpler loop without end-wall effects (mean line and compressor dynamics calculation at each optimization iteration). In the second optimization strategy, end-wall effects are applied to the optimized compressor only once, at the end of the optimization process. This strategy has the advantage of being computationally less expensive than the first one.

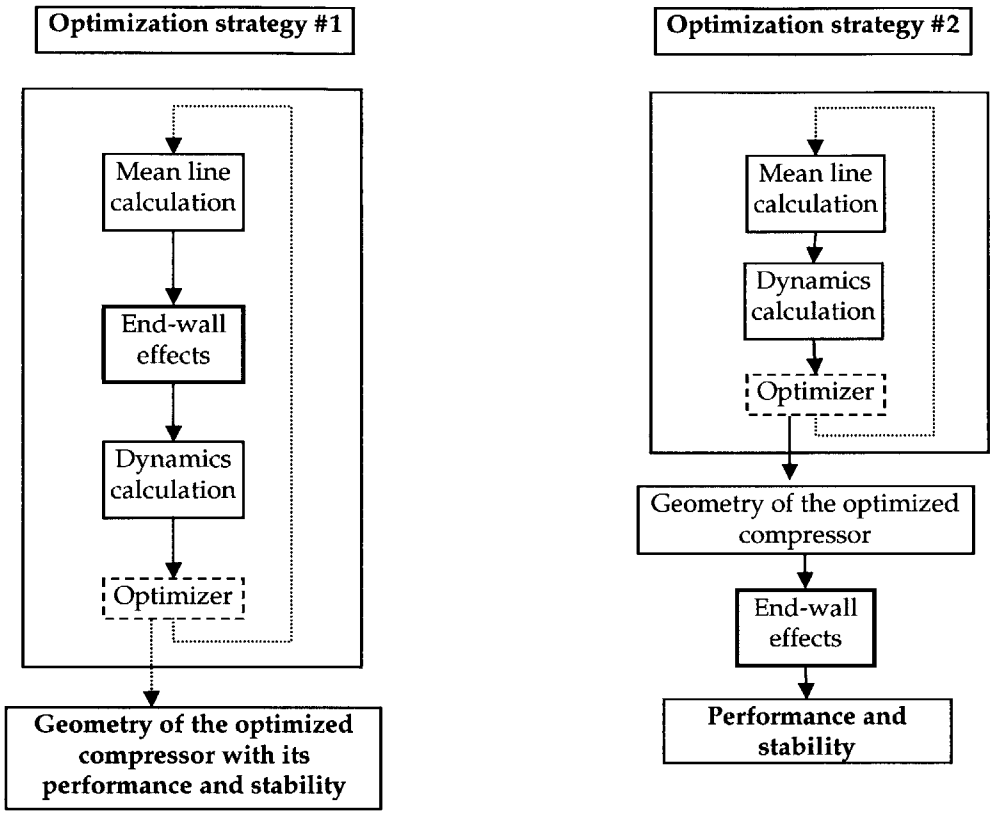

Figure 5-4: Sketch presenting two possible optimization strategies.

Figure 5-5 suggests that strategy #1 should be used. This figure presents the difference between pressure ratios, efficiencies and stall margins, computed with and without end-wall effects, as functions of Δ_{bc}. The curves plotted in Figure 5-5 would show a constant value if the changes in Δ_{bc} did not impact the end-wall effects. In a situation where end-wall effects are not affected by Δ_{bc}, optimization strategies #1 and #2 would lead to the same geometry for the optimized compressor. Figure 5-5 shows that this is not the case: the curves do not show constant values. Hence, the end-wall effects have to be included in the calculation loop as presented in optimization strategy #1.

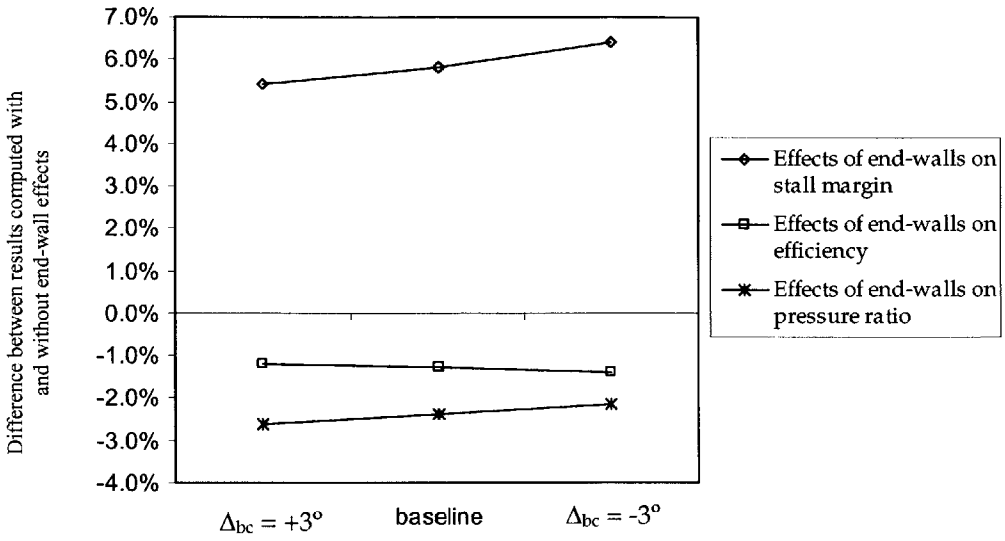

Figure 5-5: Dependency of the difference between results computed with and without end-wall effects on the angle of blade channel modification Δ_{bc}.

5.3 Conclusion

In this chapter were discussed and quantified the effects of a blade channel modification on performance and stability. The main conclusion is that a positive Δ_{bc} leads to a decrease in diffusion factor entailing an increase in stability and a lower performance. Furthermore, two sensitivity analyses were performed involving profile loss only or profile and end-wall loss. These sensitivity analyses led to the determination of the effect that modifications of the blade channel angle have on performance and stability. The optimization strategy was devised, thus, the optimization loop presented in Figure 2-1 is used in Chapter 6 for the optimization. The range of evolution of the design variables is also defined: [-3° ; +3°] is a good interval for the blade channel modification to be used in the optimization.

Chapter 6

Preliminary Design Optimization of a 3-Stage Repeating Stage Compressor for Enhanced Stability

All the necessary components in the optimization are now assembled according to the framework presented in Chapter 2. The steps leading to the choice and implementation of the blade channel modification linked to modifications of the blade-row losses were developed in Chapters 3, 4 and 5. This chapter aims at demonstrating the compressor design optimization for enhanced stability, i.e. proving that this conceptual idea is feasible. The 3-stage repeating stage compressor defined in Appendix B is to be optimized.

This chapter first summarizes the optimization objectives and design variables. The optimization details are then presented: the algorithms used are explained and the definition of a multi-objective problem is given. Finally, optimization results are presented and discussed, leading to design implications and limitations.

6.1 Presentation of the Objectives and Design Variables of the Optimization

The objective functions of any optimization are quantities that are to be maximized (or minimized, depending on the context). These quantities describe the fitness of the designs generated at each step of an optimization process.

The objective functions of this work are, as presented in the introduction, the performance of a given axial compressor as well as its dynamic stability. Obviously, to be able to measure the fitness of

a given compressor in the light of this optimization, metrics for both performance and stability are needed.

First of all, to measure compressor performance, two thermodynamic quantities are chosen: overall pressure ratio and adiabatic efficiency.

The determination of the onset of instability is a challenging issue. So far, a real metric for stability based on a dynamic compression system model has not been defined. Current research carried out by Dorca [4] aims at defining such a metric. Because of time constraints, however, a common metric for stability is adopted here for the optimization: stall margin. This metric is widely used in industry to measure the stability margin of a gas turbine engine. In spite of not being the most stringent one and not making the most of all the information provided by the dynamic calculation (refer to Dorca [4]), this metric has several advantages. It is easy to implement, and is meaningful to engineers working on compressors. NASA's definition of the stall margin is used and tts expression is given below. Stall margin is computed with flow information at the stall point and the working point:

$$SM = 1 - \left[\frac{\Pi_{\text{working point}}}{\Pi_{\text{stall point}}} \cdot \frac{\dot{m}_{\text{stall point}}}{\dot{m}_{\text{working point}}} \right].$$

It is recalled here that, as presented in section 2.3, the stall point is determined based on the dynamic system modeling. The stability of the least stable mode found from the dynamics calculation is the criterion for stability.

To summarize, the optimization to be carried out is a multi-objective problem using pressure ratio, efficiency and stall margin as the three objective functions.

To achieve an optimization of the objectives, the design variables are geometric design variables (blade channel modification, as presented in Chapter 4) influencing the diffusion and hence performance (quantified in terms of stagnation pressure loss) of each blade-row. Thus, for a three-stage compressor, 6 design variables (one per blade-row) have to be adjusted by the optimizer.

6.2 Optimization Details

This part introduces the optimization tool used in this research. It also presents how the optimization is set up and what algorithms and methods are used.

It is recalled that the software used for the present research is Isight version 7.1 Beta. This is an academic version, limited to 8 design variables.

6.2.1 Algorithms

Two main types of algorithms are used in optimizations for design purposes: gradient-based methods and heuristic methods. Both are implemented in this research to get to the optimized geometry of a given compressor, and both are briefly described hereafter.

Gradient-based Methods: Sequential Quadratic Programming

Gradient-based methods are, as indicated by their name, based on the calculation of derivatives. Once an objective function is defined, information about its gradients is used to iterate and converge to an optimum (that can be either *the* global optimum or *a* local optimum). The gradient-based method used in this thesis is called SQP (Sequential Quadratic Programming). It is well-suited for constrained and non-linear optimizations, and is widely used in engineering applications. It can be used for the purpose of this research: the compressor optimization for enhanced stability is constrained and the relation between the design variables (the shapes of loss buckets) and the objectives (performance and stability) is non-linear.

The principle of SQP is briefly reviewed here (for more details, refer to Willcox [17]). A standard definition for a general optimization problem is first given:

$$\min J(\mathbf{x}),$$

subject to $g_j(\mathbf{x}) \leq 0 \quad j = 1,...,m_1$ and $h_k(\mathbf{x}) = 0 \quad k = 1,...m_2$ with $\mathbf{x}_i^{\text{lower}} \leq \mathbf{x}_i \leq \mathbf{x}_i^{\text{upper}}$

where $\mathbf{x}$ is the vector of design variables and $J(\mathbf{x})$ the objective function to be minimized, $\mathbf{g}$ and $\mathbf{h}$ are the inequality and equality constraints.

Gradient search methods are iterative procedures: from a given initial design vector $\mathbf{x}^0$, the algorithm determines at each step a search direction $\mathbf{S}$ and a distance α from the design vector at the previous iteration:

$$\mathbf{x}^q = \mathbf{x}^{q-1} + \alpha^q \mathbf{S}^q.$$

The optimization process can be sketched as shown in Figure 6-1.

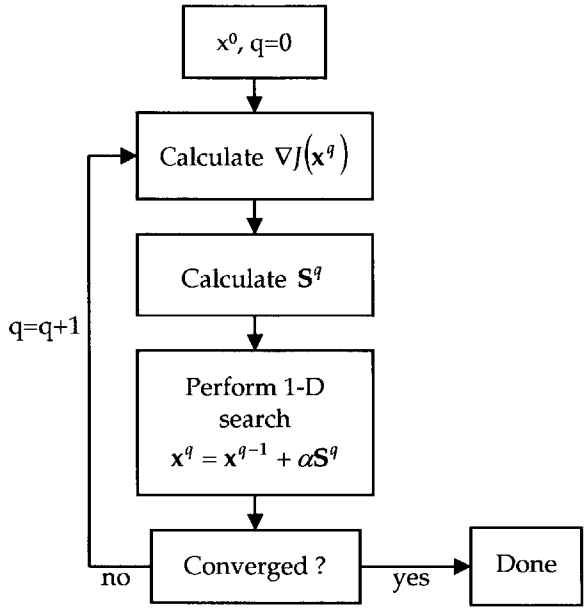

Figure 6-1: Sketch presenting the iterative process for a gradient-based algorithm (adapted from [17]).

SQP is called a quadratic method since it uses at each step a quadratic approximation to the Lagrangian function defined as:

$$L(\mathbf{x},\lambda) = J(\mathbf{x}) + \sum_{j=1}^{m_1} \lambda_j g_j(\mathbf{x}) + \sum_{k=1}^{m_2} \lambda_{m_1+k} h_k(\mathbf{x}),$$

where λ_j are called the Lagrange multipliers.

The main drawback of this method is that, like any gradient-based search, it is likely to get locked in a local optimum. The optimization strategy presented later and used for this research can however be implemented to deal with this issue.

Heuristic Techniques: Genetic Algorithm

Heuristic methods are techniques using a combination of randomness and heuristic rules to guide the search for global maximum or minimum. The heuristic method used in this research is the Genetic Algorithm (GA). The principle of this type of method is as follows: a possible design of a given system – as represented by its design vector $\mathbf{x}$ – can be considered as an individual fighting for

survival within a larger population. Natural selection is a very successful principle of organization for optimizing a population of individuals. Only the fittest individuals (fitness is assessed via objective functions) survive along the process of evolution. The basic parameters that have to be chosen to perform a GA are:

- The population size: it determines the number of individuals belonging to each generation.
- The number of generations: it determines how long the evolution process lasts. After a specified number of generations, the evolution process stops and the fittest individual is kept as the optimized solution.
- The mutation rate: randomness is introduced in the evolution process as it is in the process of natural evolution when mutations happen. The frequency of random changes introduced in designs depends on the mutation rate. A 1% mutation rate means that the probability of a random change in a bit (coding the characteristics of a design) is 1/100.

GAs are powerful methods because they allow designers to explore the entire design space contrary to gradient-search methods that follow the path indicated by gradient-based information and that can get locked in local maxima. Furthermore, in contrast with gradient-based methods where the solutions depend on the initial condition of the search algorithm, GAs can be started from any random initial condition. On the other hand, the main disadvantage of GAs is that they are computationally intense and their application for optimization problems with large numbers of design variables can turn out to be very expensive.

Optimization Strategy

Experience shows that a good strategy to be used for an optimization process is a combination of gradient-based and heuristic methods. For example a GA can be used first to approach the optimal solution, enabling a wide exploration of the design space. Then SQP can be used to explore the neighborhood of the solution found by the GA to try and improve it further. The fact that the SQP starts from the GA's solution, thus closer to the optimal solution, makes it less likely for the algorithm to get trapped in a local optimum.

6.2.2 Multi-Objective Problem: Weighted Sum Approach

As already explained, the inputs to the optimizer are the compressor performance and stability and the outputs, the new loss buckets coefficients. The optimization to be performed is inherently

multi-objective, since pressure ratio, efficiency, and the metric for stability (stall margin) are the three objectives. To deal with this problem, a weighted sum approach is performed as shown below.

$$J = \lambda_1 \cdot \frac{\Pi}{\Pi_{ref}} + \lambda_2 \cdot \frac{\eta}{\eta_{ref}} + \lambda_3 \cdot \frac{SM}{SM_{ref}}.$$

$J\left(\Pi/\Pi_{ref}, \eta/\eta_{ref}, SM/SM_{ref}\right)$ is the objective function that has to be maximized. The reference values are used to scale the individual objectives. It is obvious that a simple addition of a pressure ratio (typically 2) and of a stall margin (typically 0.2) would give more weight to the pressure ratio simply because of the respective orders of magnitudes: any improvement in stall margin would be outweighed by the numerical value of the pressure ratio. The scaling (or reference) values are typically baseline levels of the performance and stability metrics.

In addition to the scaling, it is also possible to weight the objective, with weighting coefficients λ_i. This is obviously a choice up to the designer, and it can be changed if more (or less) emphasis is to be given to stability (or performance). This is nonetheless an important choice as the final design will heavily depend on the weighting function chosen before the optimization starts (a parametric study is performed in section 6.3.4). The solution towards which the optimizer will converge, on the Pareto front, depends on the respective weight distribution.

6.3 Proof of Concept: Results and Discussion

A compressor design optimization for enhanced stability is carried out on the 3-stage, repeating-stage compressor and is used as the proof of concept of the framework introduced.

6.3.1 Formal Formulation of the Problem

A formal formulation of the optimization problem is given below, summarizing what the design vector, objective function, constraints and bounds are. The parameters defining the problem have to be chosen carefully to avoid non-physical optimization results. Poor physical insight is maybe a drawback of the optimization algorithms: if the designer is not careful while constraining the objectives and design variables, experience shows that a deficient definition often leads optimizers to find unreasonable solutions. The algorithms lack physical insight of the systems they deal with; they only follow gradient or fitness information to direct their search.

The optimization problem is defined as follows:

Design Variables:

$$\mathbf{x} = \left[\xi_0^1 \quad \cdots \quad \xi_0^3 \quad \cdots \quad \xi_0^6\right]^T,$$
$$subject\ to \quad 0.8 \le \xi_0^i \le 1.2,$$

where ξ_0^i is the coefficient to be applied to the corresponding loss bucket, for blade-row i (the first blade-row is rotor 1, the second is stator 1, the third is rotor 2, etc.). It is recalled that, as explained in Chapter 4, the specification of ξ_0 determines the set (ξ_0, ξ_1) equivalent to a given Δ_{bc} (the bounds 0.8 and 1.2 for ξ_0 correspond to the bounds -3° and +3° for the modifications of the blade channel angle Δ_{bc}).

Multi-Objective Function:

The multi-objective function is

$$\mathrm{J} = \frac{\Pi}{\Pi_{ref}} + \frac{\eta}{\eta_{ref}} + 2 \cdot \frac{SM}{SM_{ref}},$$

where the reference values were set to the baseline values, that is $\Pi_{ref} = 1.317$, $\eta_{ref} = 0.924$ and $SM_{ref} = 0.267$.

The weighting of the stall margin λ_3 is set to 2 whereas the weights of the pressure ratio and efficiency λ_1 and λ_2 are set to 1. This choice was motivated by the necessity of the objective vector to contain two metrics for performance and only one for stability. Using the same weight for all of them would lead to an overweighting of performance to the detriment of stability. In order to restore a balance, the set of weighting coefficients proposed is chosen. The influence of the weighting coefficients is further discussed in section 6.3.4.

Constraints:

The following constraints are imposed on the objectives along the optimization process:

$$0.23 \le SM$$
$$1.291 \le PR$$
$$0.905 \le \eta$$

These constraints are imposed in order to direct the optimizer to reasonable solutions: first, to limit the performance loss to small values (less than 2% of the baseline value for pressure ratio and efficiency). Second, the stall margin is constrained to stay above 23% (common stall margins in industry world are in the vicinity of 25%).

These constraints constitute a realistic problem formulation: a first analysis is carried out on a baseline compressor to estimate its performance and stability. Then, with pre-defined performance targets, it is decided to try and improve stability as much as possible without altering performance beyond pre-set limits.

6.3.2 Algorithm Settings

This section presents the SQP and GA settings used to carry out the optimizations.

In terms of algorithms parameters and step details used, the default settings proposed by Isight were applied for the SQP: that is a forward finite difference method with a relative gradient step of 10^{-4}.

Concerning the GA, the multi-island algorithm was used with the following settings: a single island, population size of 35 individuals, 35 generations and a 4% mutation rate. The mutation rate was set to 4% since experience shows that this is a relevant value. A compromise is reached between randomly introduced diversity and no diversity at all, leading to a good convergence speed. Too high mutation rates entail too much randomness introduced in the process, hence poor convergence or even no convergence at all. On the other hand, when mutation rates are too low, very slow convergence speeds are achieved and a poor exploration of the design space is performed.

6.3.3 Optimization Results

The optimization results are presented, and the type of strategy (that is the optimization algorithm) is specified together with the details of the calculations.

Calculation #1 was carried out using a SQP method only. The starting point was the baseline configuration. 231 iterations were performed and the computation lasted 45 minutes.

Calculation #2 was carried out with a GA. 1225 iterations were performed and the computation took 210 minutes.

Calculation #3 was carried out with a SQP method only. However, the initial point for the computation was the result provided by calculation #2. 217 iterations were performed and the computation lasted 43 minutes.

The results of these three calculations are summarized in Table 6-1.

Calculation #	OPR		Efficiency		Stall margin		Objective	
Baseline	***1.317***		***0.924***		***26.7%***		***4.0***	
1	1.291	-2.0%	0.919	-0.5%	33.0%	+6.3	4.449	+10.1%
2	1.291	-2.0%	0.919	-0.5%	33.1%	+6.4	4.454	+11.35%
3	1.291	-2.0%	0.919	-0.5%	33.1%	+6.4	4.454	+11.35%

Table 6-1: Results of the optimization calculations.

The overall optimization result is satisfying: all the calculations lead to an improvement of the stall margin with a minimal loss in performance.

The best solution is found by the GA (calculation #2) with an overall objective function improvement of 11.35%. The strategy presented in section 6.2.1 (i.e. a gradient-based optimization with a starting point using a geometry provided by the GA's solution) did not further improve the optimized compressor given by calculation #2 (the solution was improved by less than 0.01%). However, one can be confident that the objective function of the optimized compressor reached not only *a local* maximum, but *the global* maximum since no further improvement could be achieved. No other combination of loss coefficients would yield a better compressor (better in terms of objective function).

Furthermore, the strategy that consists of applying an SQP-based optimization combined with a GA seems to be useless from the example presented here. However, this is not always the case as it allows one to know whether the GA converged or not. The SQP searches in the neighborhood of the GA's best solution for further improvement: if none is observed, the GA converged.

Obviously, for the 3-stage compressor optimization, calculation #1 is not to be discarded since it finds an acceptable solution (acceptable meaning only 0.1% below the best solution in terms of stall margin for the same performance) in a limited number of iterations (5 times less iterations than the GA). For large-scale optimizations involving a high number of design variables, it is arguable why a direct SQP could be preferred to an expensive GA since SQP can lead to appreciable time savings as demonstrated here.

The last comment that can be made is that the constraint imposed on the pressure ratio is active, meaning that the constraining value is reached. This means that if that particular constraint is modified, the final solution found will be different. The constraining value was chosen to limit performance loss.

Using optimization tools in industry, designers will start the process with a clear objective in mind such as: "stability has to be improved with less than 2% performance loss", or else: "stability has to be improved by 5% with the minimum performance loss achievable". Such objectives define the constraints to be applied to the problem.

The final (i.e. optimized) geometry is now presented with more details. The blade channel modification angles computed (calculation #2) for the blade-rows of the optimized compressor are presented in Table 6-2. Diffusion factors and turnings for the baseline compressor and the optimized compressor are given in Table 6-3. The results illustrate the impact of the optimization on the compressor. Finally, the performance and stability modifications are summarized in Table 6-4:

Rotor 1	Stator 1	Rotor 2	Stator 2	Rotor 3	Stator 3
-0.33°	+2.63°	+2.46°	+2.40°	+1.76°	+2.70°

Table 6-2: Blade channel modifications for the optimized compressor's blade-rows.

	Rotor 1	Stator 1	Rotor 2	Stator 2	Rotor 3	Stator 3
DF baseline compressor	0.595	0.571	0.568	0.572	0.563	0.521
DF optimized compressor	**0.598**	**0.553**	**0.528**	**0.533**	**0.522**	**0.476**
Turning baseline compressor	34.014	33.351	33.013	33.019	32.985	32.874
Turning optimized compressor	**34.322**	**30.993**	**29.937**	**29.926**	**30.39**	**29.474**

Table 6-3: Diffusion factors and turning of the baseline and the optimized compressor.

OPR		**Efficiency**		**Stall margin**	
1.291	**-2.0%**	**0.919**	**-0.5%**	**33.1%**	**+6.4**

Table 6-4: Summary of the optimized compressor's performance and stability (compared to the baseline compressor).

Table 6-3 shows that the blade-rows of the optimized compressor have lower diffusion factors and lower turnings than in the baseline compressor. This leads to the reduction of the overall pressure ratio and the improvement of the stall margin.

Note that the optimization process leads to a solution that disrupts the repeating-stage pattern of this compressor. The fact that different blade metal angles variations are introduced for each blade-row leads to a non-repeating-stage compressor. However, keeping the repeating-stage scheme was not among the objectives of this optimization, but would have been achievable by constraining the design variables to take equal values for all the blade-rows.

Figure 6-2 presents the blade-row loss buckets of both the baseline and optimized compressors. The increase in the blade channel angles for all the blade-rows (except for rotor 1) leads to:

- a performance penalty since the loss levels are higher at the design point,
- a stability enhancement since the increase (in absolute terms) in loss slopes occurs at a lower flow coefficient.

It is furthermore unexpected to see that a negative blade channel modification is imposed on the compressor's first rotor. However, the performance constraint may explain this trend: a positive blade channel modification would lead to an altered pressure ratio resulting in the violation of the lower constraint on that objective. The importance of using optimization algorithms is enlightened as a designer would probably not think of reducing a blade-row's operating range in order to improve the overall stability of a compressor.

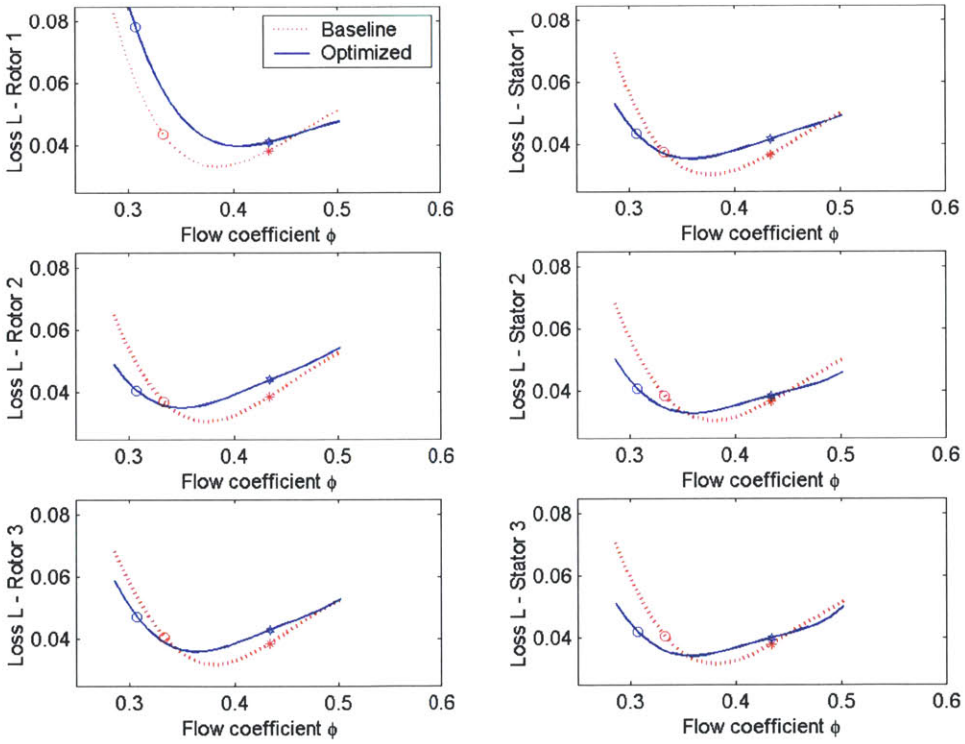

Figure 6-2: Blade-row loss of the baseline and optimized compressors.

Figure 6-3 shows the characteristics of the baseline compressor and of the compressor optimized for stability, indicating the performance loss and stability enhancement.

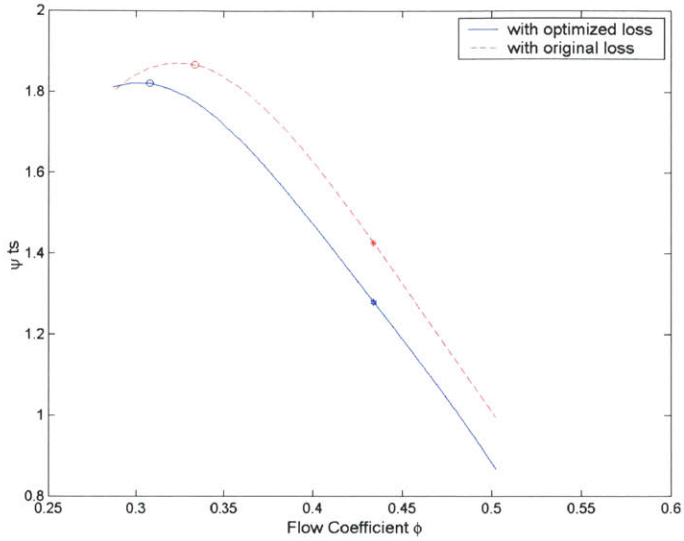

Figure 6-3: Compressors characteristic of the baseline and optimized configurations.

Finally, Figure 6-4 presents the flow path modification: the blades of the baseline compressor and of the compressor optimized for stability are drawn. Figure 6-4 enables the visualization of the design modifications brought to the baseline compressor.

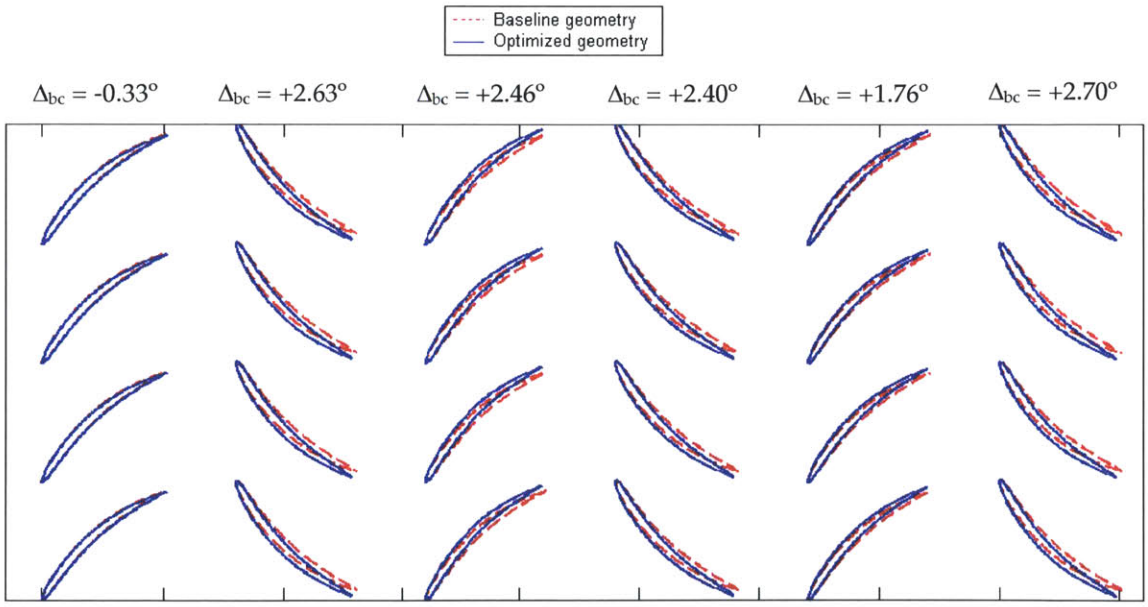

Figure 6-4: Blade passage geometries before and after the optimization.

6.3.4 Parametric Study on the Weights Used in the Objective Function

Finally, the importance of the weight distribution in the objective function is illustrated. A parametric study is performed: several optimizations are carried out with different values of weight λ_1 applied to the non-dimensional stall margin (using the objective function defined in section 6.2.2). For the sake of time, the algorithm used for all these optimizations is the SQP and not the computationally expensive GA. λ_1 is progressively decreased from an original value of 10 to 0. Each case leads to a different compressor with a different performance and a different level of stability.

	λ_1	λ_2	λ_3	OPR	η	SM
Case #1	10	1	1	***1.291***	***0.919***	***32.7%***
Case #2	2	1	1	***1.291***	***0.919***	***33.0%***
Case #3	1	1	1	***1.291***	***0.920***	***32.5%***
Case #4	0.5	1	1	***1.318***	***0.924***	***26.7%***
Case #5	0	1	1	***1.343***	***0.923***	***23.1%***

Table 6-5: Results of optimizations carried out on objective functions with different weight distributions.

It is interesting to analyze the different cases with respect to case #2, since in the last section the optimization was carried out with this weight distribution. Case #3 gives less importance to SM than in case #2 as λ_1 is set to 1. The optimized compressor has a better efficiency (0.920 versus 0.919) and a lower stall margin (32.5% versus 33%). Decreasing further λ_1 (in cases #4 and #5) leads to optimized solutions with higher performance and lower stall margin as expected. Case #5 is an optimization for pure performance as λ_1 is set to 0. The compressor obtained from case #3 has a pressure ratio 2% higher than the baseline compressor.

Case #1, where λ_1 is set to 10, leads to a lower stall margin than obtained from case #2 although at least the same level of stability could have been expected from case #1 and case #2. In these two cases, the constraint imposed on the pressure ratio ($1.291 \leq PR$) prevents the optimizer from improving further the stall margin since any increase in SM would lead to a decrease in pressure ratio. Furthermore, case #1 shows the importance of a careful choice of the weight distribution. Increasing indefinitely λ_1 will not necessarily yield a better solution in terms of stall margin. When λ_1 is modified, the topology of the objective function changes as well, and the SQP, led by gradient information, follows a different path ending on a solution worse than the solution of case #2 in terms of stall margin.

6.3.5 Conclusions

The optimization of the 3-stage, repeating-stage compressor shows an implementation example of the framework introduced in this thesis. Enhanced stability is achieved minimizing the performance penalty for the baseline compressor.

It has to be kept in mind that the optimization presented in this chapter is a proof-of-concept: it proves that the conceptual idea of optimizing a compressor for enhanced stability is feasible. The limitations of the model used (in particular in terms of loss interpolation, as seen in Chapter 5) and the small magnitudes of the changes in performance (less than 2% performance drop from the baseline compressor) indicate that the step from a proof-of-concept to a real optimization cannot be done. However, the optimization carried out on a generic compressor showed the possibility of improving the stall margin by making modifications to the compressor geometry that are simple to implement. For cost reasons, engine manufacturers are not inclined to design new blade profiles. The changes proposed in this thesis simply involve blade re-staggering, blades being hinged at their leading edge. In spite of their simplicity, the geometric changes can significantly improve compressor stability (6.5% more stall margin for the optimized 3-stage compressor).

Concerning the optimization details, a strategy involving a genetic algorithm (possibly combined with a SQP) yields the best solution. Although GAs are computationally more intense than gradient-based methods, they usually enable a better exploration of the design space, often leading to better solutions (as long as time is not limited). It was finally proved that the results depend on the way the problem is formulated: a modification of the weight distribution in the objective function leads to different compressors, as shown by the parametric study carried out in section 6.3.4. There is not one single answer to any stability enhancement problem; depending on the requirements, hence on the constraints and weight distributions, optimizations lead to different compressor configurations.

Chapter 7

Conclusions and Future Work

7.1 Summary and Conclusions

One of the objectives of this thesis was the assessment and analytical description of the relation between blade-row loss and blade-row geometry, and the impact of geometric modifications on compressor performance and stability. Possible geometric modifications to be used in the optimization framework focusing on stability enhancement were introduced. The blade channel modification was implemented in the optimization framework since it complies with the requirements imposed: firstly, it is an efficient and simple way to alter compressor stability, secondly it can be parameterized with a low number of design variables dictated by the limitations of the optimization software used in this thesis.

The main objective of this thesis was to develop and implement an inverse-design optimization tool aimed at optimizing an axial compressor for enhanced stability. For this purpose, an optimization framework was conceived and implemented, linking together a mean line calculation, an unsteady compressor model based on dynamic compression system modeling, and modules calculating end-wall effects and blade-row loss.

A methodology comprised of several steps was adopted to implement the optimization framework aiming at the enhancement of compressor stability. These steps are summarized below.

- The first step to be performed is a CFD analysis (e.g. MISES), preliminary to the implementation of the optimization loop. It aims at finding a solution to the inverse-design problem that consists of establishing an analytic relation between a blade-row geometric modification and the corresponding loss modification. The interpolation of computed data allows for a simple analytic solution to the inverse-design problem.

- The second step is a sensitivity analysis aimed at quantifying the performance and stability changes incurred by the modification of the blade-row geometry. This analysis is necessary to determine the bounds on the design variables to be used in the optimization process as well as to elucidate the physical effects triggered by the geometric modifications.
- The third step is the definition of the optimization problem. This step is certainly the most important because it directly influences the final result towards which the optimization algorithms will converge. The optimization problem entails three important considerations: the definition of an objective function using the weighted sum approach (i.e. the choice of the scaling and non-dimensionalizing factors), the definition of the bounds on the design variables, and the constraints imposed on the objectives.
- The final step is the optimization per se where the strategy to be used has to be chosen. It was shown that if severe limitations are imposed in terms of computational time, an SQP-based optimization is the most efficient approach to a compressor optimization problem for enhanced stability.

One can understand from all the steps needed to implement the optimization that the framework is far from being an automated process: great care has to be taken during all the necessary steps. The simulation models need to be as accurate as possible and the problem has to be defined as precisely as possible.

Finally, a proof-of-concept was performed on a generic 3-stage, repeating-stage axial compressor, demonstrating the feasibility of the conceptual idea of designing a compressor for enhanced stability. The stall margin was improved by 6.4% while the overall pressure ratio loss was limited to 2% and the loss in efficiency was limited to 0.5%. This stability enhancement was achieved with modifications of the blade channel angles ranging between -0.3° and 2.7°, suggesting that a simple and limited geometric modification can lead to appreciable stability enhancements.

7.2 Future Work

This thesis constitutes a first step towards compressor design optimization for enhanced stability based on dynamic compression system modeling. There are many things that call for improvement and additional work needs to be conducted.

- First is the implementation of a new metric for stability, for instance as defined by Dorca [4]. The optimization could then lead to different compressor configurations taking advantage of the information provided by the dynamic compressor model.

- Second is the extension of the optimization to a higher number of design variables. This can be enabled by using another version of the Isight optimizer. A higher number of design variables would enable more geometric modifications of the blades, and hence potentially higher stability improvements by further broadening the design space. This future work could potentially lead to improved results and facilitate design tools to be used in a realistic compressor environment.
- Third is an improved search method locating the relevant eigenvalues. As soon as one wants to map out the system eigenvalues, the computational time involved can become deterring. A numerical target has to be specified in order to search for the eigenvalues in the right-hand side of the complex plane. Hence, the determination of the location of the least stable eigenvalue can be challenging when geometric parameters such as inter-gap lengths or blade metal angles are modified. The eigenvalue search is difficult since the target stays unchanged along the optimization process but the eigenvalues migrate due to the geometric modifications applied to the compressor. This can lead to computational problems that have to be dealt with in each case, reducing the robustness of the optimization framework. In a future effort, a more efficient description of the model such as a state-space model could be used to facilitate fast and simple determination of the eigenvalues. This could enable the use of more geometric design variables in the optimization process without involving expensive computational times.

Appendix A

Mean-Flow calculation

A brief description of the mean-flow calculation used in the optimization loop is given below. Some notations are repeated here together with the governing thermodynamic equations.

Calculations are performed at a mean radius, chosen to be the Euler radius splitting the compressor mass flow into equal parts below and above of this radius:

$$R_{mean} = \sqrt{\frac{\left(R_{tip}^2 + R_{hub}^2\right)}{2}}$$

Figure A-1 presents in more detail the notations of velocities and angles used in the mean-flow calculation:

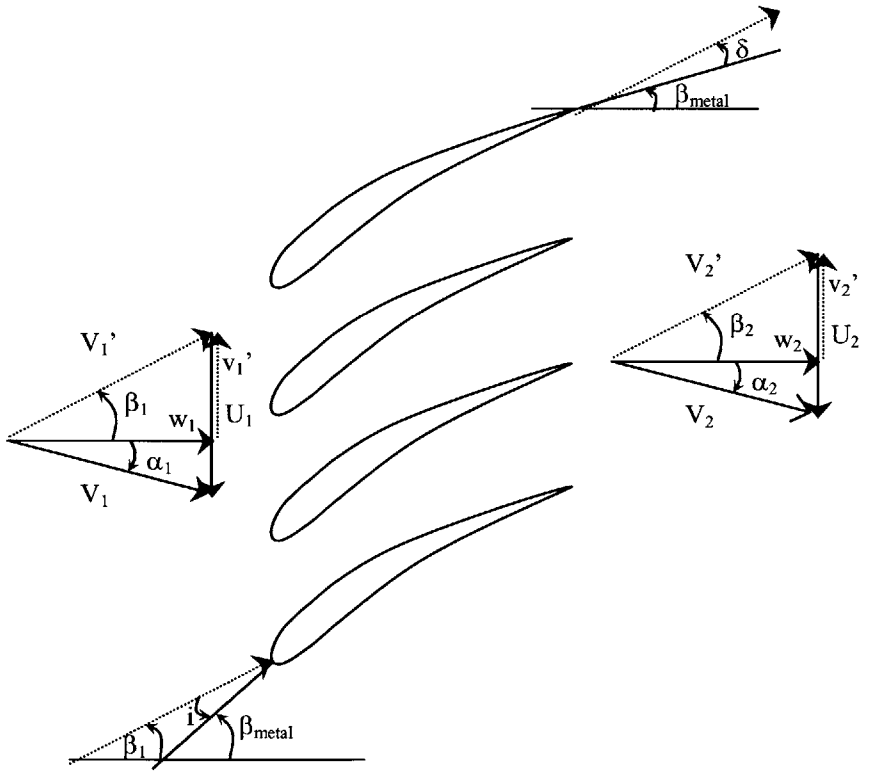

Figure A-1: Definition of angles and notations used in the mean line calculation.

Finally, the main scheme adopted for the compressible calculation is presented in the following sketch:

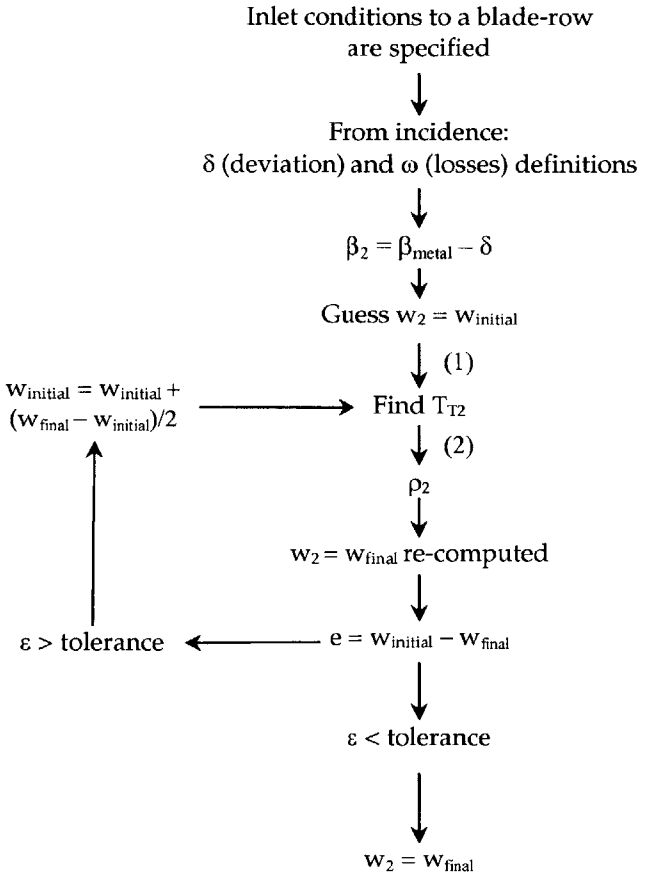

(1) To determine the total temperature at the blade-row exit from the axial velocities, the Euler turbine equation is used:

$$c_p(T_{t2} - T_{t1}) = \omega(r_2 v_2 - r_1 v_1).$$

(2) The density at the blade-row exit is computed using velocity triangle relations as well as relations between total and static temperatures and pressures:

$$T_t = T + \frac{V^2}{2c_p},$$

$$\frac{P_t}{P} = \left(\frac{T_t}{T}\right)^{\frac{\gamma}{\gamma-1}}.$$

Finally, the total pressure loss is accounted for using:

$$\omega = \frac{P'_{t2\,isentropic} - P'_{t2}}{P'_{t1} - P_1}.$$

From this relation, the total pressure at the exit of the blade-row then yields:

$$P'_{t2} = P'_{t2\,isentropic} - \omega\left(P'_{t1} - P_1\right).$$

Appendix B

Geometry and operating conditions of the 3-stage, repeating-stage compressor

This appendix presents the geometry of the compressor used throughout this thesis. This geometry is input to the mean line calculation briefly described in Appendix A.

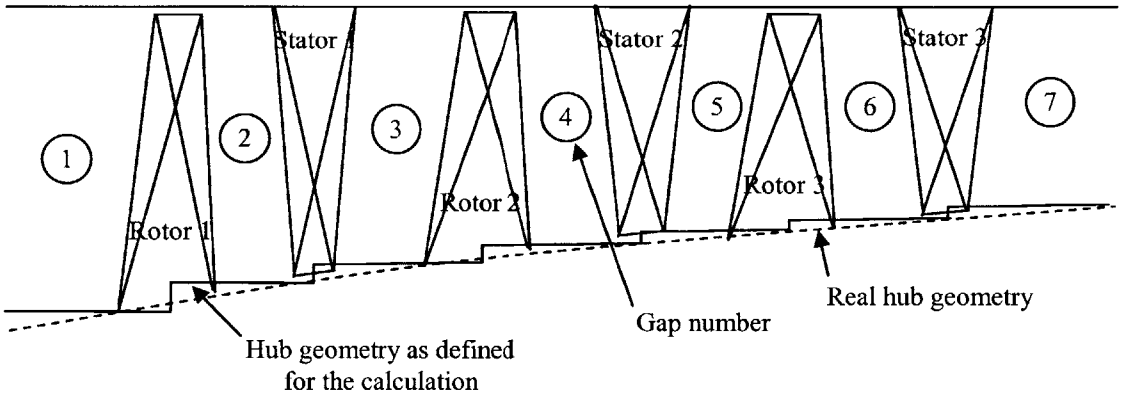

Figure B-1: Sketch presenting the gaps numbering used in the mean line calculation as well as the duct geometry

Gap-length [m]	.25	0.005	0.005	0.005	0.005	0.005	0.25
Tip radii of the blade rows [m]	0.2591	0.2591	0.2591	0.2591	0.2591	0.2591	0.2591
Hub radii of the blade rows [m]	0.2268	0.228	0.2295	0.2305	0.2315	0.2325	0.2353

Table B-1: Duct geometry of the 3-repeating-stage compressor

	Chord [m]	Stagger [°]	Inlet metal angle [°]	Outlet metal angle [°]
Rotor 1 to 3	0.015	42	59	25
Stator 1 to 3	0.015	42	59	25

Table B-2: Blades geometry of the 3-repeating-stage compressor

The operating conditions used for the calculations were the following:

Mass flow for the specific calculation case [kg/s]	3.3
Universal gas constant [J/kg.K]	287
Specific heat at constant pressure [J/kg]	1004.5
Ambient static pressure [Pa]	101300
Ambient static temperature [K]	288.15
Ambient static density [kg/m^3]	1.225
Rotation speed [rad/s]	525.57
Inlet swirl angle [°]	25

Table B-3: Operating conditions of the 3-repeating-stage compressor

Bibliography

[1] BLANVILLAIN, E., *"Dynamic Stability Analysis of a Multi-Stage Axial Compressor with Design Implications"*. Master of Engineering thesis, Department of Aeronautics and Astronautics, MIT, 2003.

[2] BUCHE, D., GUIDATI, G., STOLL, P., *"Automated Design Optimization of Compressor Blades for Stationary, Large-Scale Turbomachinery"*. GT2003-38421. In *Proceedings of the ASME Turbo Expo 2003.*

[3] CUMPSTY, N., *"Compressor Aerodynamics"*. Addison-Wesley Publishing Company, 1989.

[4] DORCA, J. M., *"An Energy-Like Stability Metric and Design Criterion Based on Axial Compressor Dynamics"*. Master's thesis, Department of Aeronautics and Astronautics, MIT, 2003.

[5] DRELA, M., *"XFoil"*, http://raphael.mit.edu/xfoil/.

[6] GREITZER, E.M. "Stability *of Pumping Systems – The 1980 Freeman Scholar Lecture"*, Journal of Fluids Engineering (Jun. 1981), Vol. 163, pp. 193-240.

[7] GREITZER, E.M. *"REVIEW – Axial Compressor Stall Phenomena*, Journal of Fluids Engineering (Jun. 1980), Vol. 102, pp. 134-150.

[8] KERREBROCK, J., *"Aircraft Engines and Gas Turbines"*, The MIT Press, Cambridge, Massachusetts, 2001.

[9] LAVAINNE, J., *"Sensitivity of a Compressor Repeating Stage to Geometric Variation"*. Master's thesis, Department of Aeronautics and Astronautics, MIT, 2003.

[10] LONGLEY, J. *"A Review of Nonsteady Flow Models for Compressor Stability"*, ASME J. of Turbomachinery (Apr. 1994), pp. 202-215.

[11] MOORE, F., AND GREITZER, E. *"A Theory of Post-Stall Transients in Axial Compressors: Part I – Development of the Equations"*, ASME J. of Engineering for Gas Turbines and Power, Vol.108 (1986), pp. 68-76.

[12] SIEVERDING, F., CASEY, M., RIBI, B., MEYER, M., *"Design of Industrial Axial Compressor Blade Sections for Optimal Range and Performance"*. GT2003-38036. In *Proceedings of the ASME Turbo Expo 2003.*

[13] SMITH, L. H., *"Casing Boundary Layers in Multistage Axial-Flow Compressors". Flow Research on Blading*, ed., L. S Dzung, Elsevier Publishing, Amsterdam, Netherlands, 1970.

[14] SMITH, L. H., KOCH, C. C., *"Loss Sources and Magnitudes in Axial-Flow Compressors". Engineering for Power*, Vol. 98, No. 3, 1976.

[15] SPAKOVSZKY, Z., *"Applications of Axial and Radial Compressor Dynamic System Modeling"*. PhD thesis, Department of Aeronautics and Astronautics, MIT, 2000.

[16] SPAKOVSZKY, Z., *"Backward Traveling Rotating Stall Waves in Centrifugal Compressors"*. ASME Journal of Turbomachinery, Vol. 125, No 4, Oct 2003.

[17] WILLCOX, K., *"Numerical Optimization II"*. Multidisciplinary System Design Optimization Class Notes, 16.888, MIT, Spring 2003.

[18] YOUNGREN, H., DRELA, M., *"A User's Guide to MISES 2.53"*. MIT Computational Aerospace Sciences Laboratory, December 1998.